TWO PERIODS OF MIOCENE TO CONTEMPORARY FLATTENING STRAIN DURING DISPLACEMENT ON A LOW-ANGLE DETACHMENT AND ON SUPERPOSED CURVED HIGH-ANGLE FAULTS, VOLCANIC HILLS, SOUTHWEST NEVADA

by

Amy R. Webber

APPROVED BY SUPERVISORY COMMITTEE:

____

Carlos Aiken, Chair

____

Thomas Brikowski

____

Ignacio Pujana

Copyright 2018

Amy R. Webber

All Rights Reserved

I would like to dedicate this thesis to my crazy loving family for all of their support and for constantly reminding me we belong outside the box.

TWO PERIODS OF MIOCENE TO CONTEMPORARY FLATTENING STRAIN DURING DISPLACEMENT ON A LOW-ANGLE DETACHMENT AND ON SUPERPOSED CURVED HIGH-ANGLE FAULTS, VOLCANIC HILLS, SOUTHWEST NEVADA

by

AMY R. WEBBER, BS

THESIS

Presented to the Faculty of

The University of Texas at Dallas

in Partial Fulfillment

of the Requirements

for the Degree of

MASTER OF SCIENCE IN

GEOSCIENCES

THE UNIVERSITY OF TEXAS AT DALLAS

December 2018

ACKNOWLEDGMENTS

I would like to thank Dr. John S. Oldow for his mentorship and his contributions to this thesis. I would also like to thank Dr. Carlos Aiken for taking over as supervising professor when Dr. Oldow was no longer available, and my committee members, Dr. Thomas Brikowski and Dr. Ignacio Pujana, for their feedback on this research project. A special thanks to the members of the Ellison Miles Geoscience Research Group, including Nick Mueller, Scott Kerstetter, David Katopody, Ann Moulding, Melissa Ng, August Ridde, Becky Aguilar, Patrick Beachner, Nicholas Reynolds, Greg Greywall, Brent Cland, Sarah Sokol, and Lauren Landreneau for all of the contributions which have been incredibly helpful and are greatly appreciated. This research was supported by Pioneer Natural Resources, National Science Foundation, and the Ellison Miles Foundation.

November 2018

TWO PERIODS OF MIOCENE TO CONTEMPORARY FLATTENING STRAIN DURING DISPLACEMENT ON A LOW-ANGLE DETACHMENT AND ON SUPERPOSED CURVED HIGH-ANGLE FAULTS, VOLCANIC HILLS, SOUTHWEST NEVADA

Amy R. Webber, MS
The University of Texas at Dallas, 2018

Supervising Professor: Carlos Aiken

The Eastern California Shear Zone (ECSZ) and central Walker Lane (CWL) form part of a tectonic boundary zone separating the Sierra Nevada and the central Great Basin. The ECSZ and CWL are misaligned and were kinematically linked by the Sliver Peak-Lone Mountain (SPLM) detachment from 13 to 4 Ma and subsequently by the active curved-array of east-northeast and north-northwest striking faults of the Mina deflection. Pliocene to contemporary transtension (constrictional strain) dominates within the ECSZ and CWL but in the Mina deflection, the geometry of individual curved fault systems results in areas of finite flattening. South of the Mina deflection in northern Fish Lake Valley, faults in the Volcanic Hills formed in the hanging wall of the curved Emigrant Peak fault zone, which truncates the SPLM detachment exposed in the footwall in the Silver Peak Range to the east. Volcanic and sedimentary rocks in the Volcanic Hills were deposited in localized basins active during displacement on the SPLM detachment. Geologic mapping, kinematic analysis, and fault-slip inversion reveal that the high-angle faults have a progressive history involving two simultaneous extension directions (flattening). A total of 392 slip lineations with shear-sense determinations were collected on all orientations of high-angle faults in the array. Slip superposition documents four extension directions separated into two successive periods, each characterized by mutually cross-cutting slip relations indicating two directions of simultaneous extension (flattening strain). The youngest system of flattening strain has a primary extension direction of west-northwest and a secondary direction of north-northeast, consistent with contemporary earthquake focal mechanisms and strain-gauge results. The older history shows east-northeast (primary) and simultaneous north-northwest (secondary) extension and is interpreted to reflect the state of strain in the upper-plate of the SPLM extensional complex.

TABLE OF CONTENTS

LIST OF FIGURES

CHAPTER 1

INTRODUCTION

The occurrence of slip vectors with different orientations on sub-parallel faults, or superposed on a single fault surface, has been documented in a diffuse zone of continental deformation in the western Great Basin. Several models account for the discrepancy in slip vectors recorded including; temporally distinct tectonic events occurring with different strain field orientations (Angelier et al., 1985; Zoback, 1989; Bellier and Zoback, 1995) and a simple shear model in which gradual deformation occurs in a right-stepping shear couple which forms centralized tectonic blocks that progressively rotate clockwise (Wesnousky, 2005). However, these models assume plane-strain conditions. In areas such as the boundary zone linking the Central Walker Lane (CWL) and Eastern California Shear Zone (ECSZ), (Fig. 1.1) a more complex geometry of structures creates a non-plane strain setting (Oldow et al., 2001; Oldow, 2003), and seemingly incompatible slip vectors analyzed assuming plane strain conditions must instead be viewed in a non-plane strain framework.

Structures that accommodate triaxial deformation, and the slip vectors associated with these structures, cannot be explained by Anderson's theory of faulting commonly applied to the structural analysis of fault patterns. In Anderson's model, two sets of conjugate fault pairs form 45° or less to the maximum compressive stress and intersect parallel to the intermediate principle strain axis (Anderson, 1951). Reches (1983), used laboratory experiments and showed rocks subjected to three-dimensional deformation produced three or four sets of mutually cross-cutting faults in a single phase arranged with rhombohedral symmetry and an equal number of distinct slip directions which also have a rhombohedral pattern. In the northern extent of the Mina deflection where right-oblique northwest trending faults of the CWL curve into east-west trending left-oblique faults (Fig. 1.1), Ferranti et al., (2009) documented finite flattening (triaxial deformation) is the result of a geometric space problem created during movement on a curved fault system which formed a prismatic basin known as Rhodes Salt Marsh (RSM). Field investigation of RSM documented mutually cross-cutting relationships between two directions of slip vectors on multiple orientations of individual fault planes.

To further Ferranti's argument for triaxial deformation, short period cyclicity of incompatible strain-axis orientations were recorded in the central Walker Lane (CWL). Over a twenty month period, the strainmeter logged two distinct strain axes that alternated between primary and secondary orientations (Ryall and Priestley, 1975). Unlike geodetic and seismological measures which are recorded on a few major faults, and on large scale magnitude strain, the strainmeter has the ability to record small scale magnitudes which probably reflect internal deformation on minor faults in structural blocks bounded by major fault systems.

In this paper, we evaluate a complex system of structures with both a curved surface expression and an orthogonal pattern near the southern extent of the Mina deflection in northern Fish Lake Valley, Nevada (Fig. 1.1) known as the southeastern Volcanic Hills (SVH). The faults exposed in the SVH are bound by a set of curvilinear faults (Emigrant Peak Fault Zone, Fig. 1.2) which are geometrically analogous to the curved fault system surrounding RSM. The system exposed in and around the SVH is superposed onto an older low-angle detachment (Silver Peak-Lone Mountain, Fig. 1.2), and high-angle faults which once soled into the structure now cross-cut the low–angle detachment fault (Ng, 2017). We use geologic mapping and fault kinematic analysis to assess the geometric and temporal relationship of extensional structures in and around

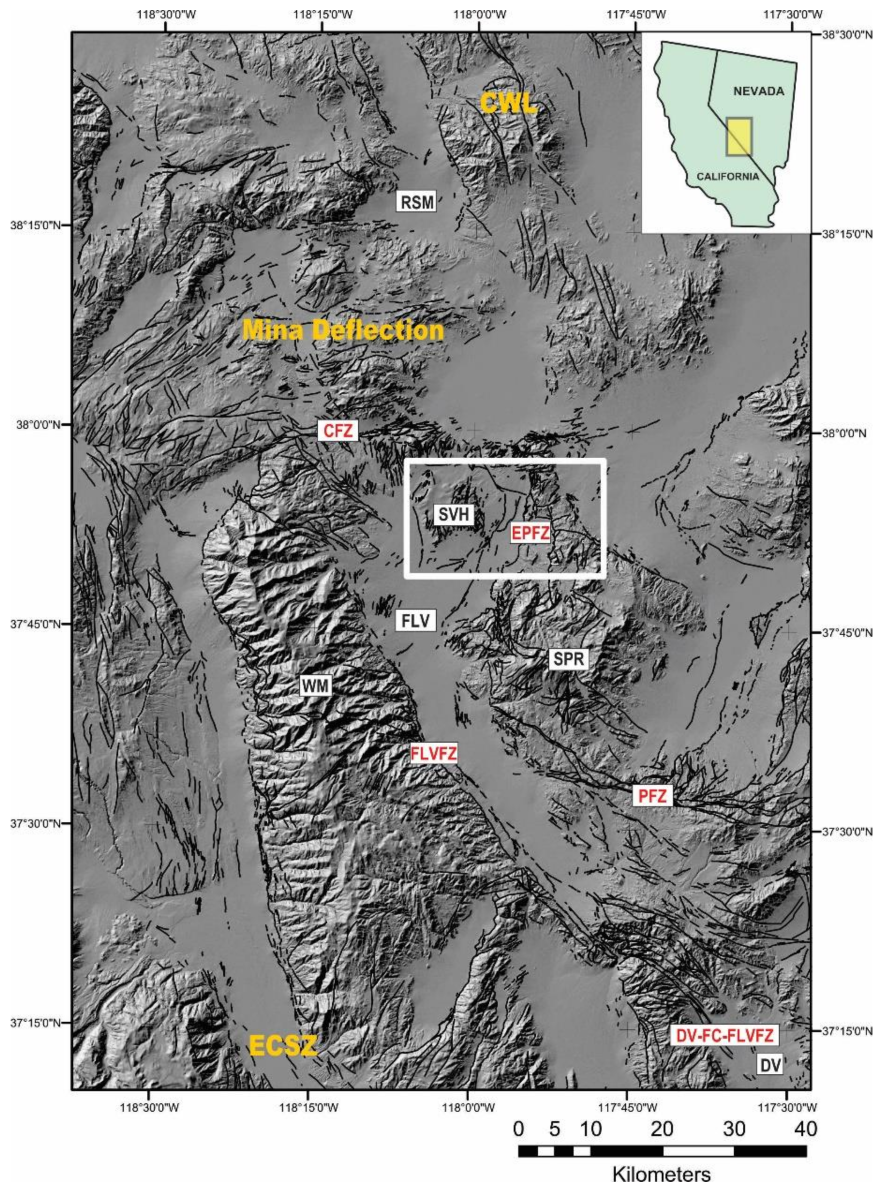

Figure 1.1. Regional hillshade map showing the major structures of the Eastern California Shear Zone and central Walker Lane kinematically linked by the Mina deflection. High-angle faults are shown in black. Physiographic locations are labeled in black, major fault zones labeled in red. Abbreviations: CFZ- Coaldale Fault Zone; CWL- central Walker Lane; DV- Death Valley; DV-FC-FLVFZ- Death Valley-Furnace Creek-Fish Lake Valley Fault Zone; ECSZ – Eastern California Shear Zone; EPFZ- Emigrant Peak Fault Zone; FLV- Fish Lake Valley; FLVFZ- Fish Lake Valley Fault Zone; RSM- Rhodes Salt Marsh; SPR- Silver Peak Range; SVH- southeastern Volcanic Hills; WM- White Mountains. White outlined box represents the study area and the location of fault geometry and 3-D Depth to basement figures.

the SVH to determine if flattening strain is a geometric requirement as down to the west displacement occurred through time.

This investigation demonstrates slip on multiple extensional faults in the SVH is compatible with non-plane strain (flattening strain), and we document four extension directions separated into two successive phases of mutually-cross cutting slip lineations superposed on to one another. We show the older history of deformation reflects the state of strain present in the upper-plate of SPLM extensional complex, whereas, the younger history is interpreted to be a result a geometrical space problem created as movement on the curved Emigrant Peak fault zone (EPFZ) occurred.

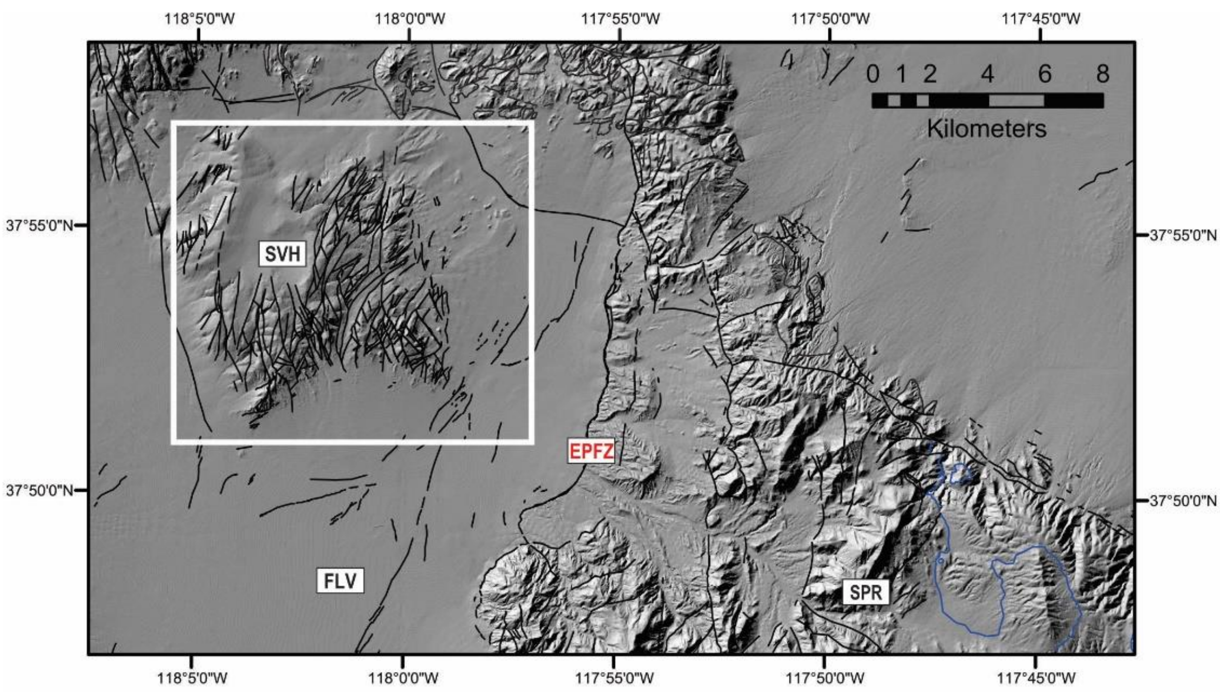

Figure 1.2. Hillshade of northern Fish Lake Valley showing the locations of structures and physiographic locations. Black lines indicate high-angle faults, blue line indicates mapped detachment, EPFZ- Emigrant Peak Fault Zone; FLV – Fish Lake Valley; SPR- Silver Peak Range; SVH- southeastern Volcanic Hills

CHAPTER 2

REGIONAL GEOLOGIC FRAMEWORK

The ECSZ and CWL form a tectonic boundary zone separating the Sierra Nevada and the central Great Basin, which accommodates differential motion between the northwest translating Sierra Nevada, and the west-northwest extending Basin and Range (Argus and Gordon, 1991; Miller et al., 2001; Oldow et al., 2001; Oldow, 2003; Bennett et al., 2003). The boundary zone consists of variably oriented faults with both transcurrent and extensional movement, which has accommodated 20-25% (10-14 mm/yr) of differential displacement between the North American and Pacific plates (Hardyman and Oldow, 1991; Oldow, 1992). The structures which constitute the boundary zone record transtensional deformation and is well documented based on seismology and contemporary global positioning system (GPS) velocities (Unruh et al., 2003; Oldow, 2003). The geometry of faults and the kinematics associated with the boundary zone have changed through time and have been kinematically linked since the mid-Miocene by a complex system of extensional stepovers (Oldow, 1992; Oldow et al., 1994, 2008, 2009; Wesnousky, 2005).

Contemporary transtensional deformation within the boundary zone began around 5-3 Ma (Oldow, 1992, 2008; Lee et al., 2009; Walker et al., 2014) and is characterized by northwest striking dextral faults of the ECSZ and CWL being linked by a 120-km long and 75-km wide system of east-northeast trending high-angle, left-oblique faults, known as the Mina deflection (Fig. 1.1). Earthquakes record right-lateral first motions on northwest striking faults and left-lateral first motions on east-west–striking faults (Doser, 1988; Rogers et al.,1991). The array of high angle east-northeast trending left-oblique faults curve at the intersections where they meet major northwest oriented structures of the CWL and ECSZ and are kinematically linked (Oldow, 1992; Ferranti et al., 2009). The northern margin of extensional complex is defined by a series of deep prismatic extensional basins that form at the apices of the curved fault arrays, including RSM (Fig. 1.1). Depths of the basins range from 0.5 to 1.5 km on the northwest trending faults to more than 3.0 km at the junction of east-northeast trending faults of the Mina deflection estimated from gravity modeling (Oldow, 1992; Stockli et al., 2003; Ferranti et al., 2009; Tincher and Stockli, 2009). The faults of the Mina deflection are underlain by a complex series of structures which previously accommodated displacement from the ECSZ to the CWL.

Pre-dating the Mina deflection, during the Miocene and early Pliocene (12-5 Ma), displacement was originally taken up further south by the Silver-Peak Lone Mountain (SPLM) extensional complex (Fig. 1.2), which linked the northwest trending Death Valley-Furnace Creek-Fish-Lake Valley Fault System in the northern ECSZ to the northwest trending faults of the southern CWL (Oldow, 1992; Oldow et al., 1994). Within the extensional complex, the northwest translating upper plate (Stewart and Diamond, 1990; Oldow et al., 1994, 2003; Kohler, 1994) exposed a shallowly northwest dipping low-angle detachment fault. High-angle faults active simultaneously soled into the detachment and created accommodation space for the deposition of Miocene volcanogenic and siliclastic rocks (Oldow et al., 2009). Paleomagnetic data indicates a 20°- 30° clockwise rotation in the extensional complex which created shortening in the upper and lower-plate rocks (Oldow et al., 2008; Petronis et a., 2009) and contributed to the growth of west-northwest trending turtleback structures. Growth of the structures ultimately locked the detachment (Kirsch, 1971) and seized the high-angle faults which controlled Miocene to early Pliocene synextensional deposition.

FLV, located to the south of the east-northeast striking faults of the Mina deflection, is an elongated northwest trending basin stretching 80 km from north to south (Fig. 1.1). To the east of FLV, the basin is bound by the Palmetto Mountains and the Silver Peak Range (SPR). The Volcanic Hills bounds the northern extent of the basin, and to the west the basin is bound by the White Mountains which are marked by the north-northwest trending Death Valley- Furnace Creek- Fish Lake Valley fault zone (DV-FC-FLFZ). The FLVFZ (Fish Lake Valley Fault Zone) is approximately 80 km long and makes up the northern most part of the DV-FC-FLVFZ which is approximately 300 km and is the longest active structure in the ECSZ (Reheis and Sawyer, 1997). At the northern end of the FLVFZ the faults distribute out into a fanned horsetail-array making up a western and eastern domain with northwest and east-northeast trending faults and east-northeast and north-northeast trending faults, respectively. Displacement across the right-lateral fault system varies in magnitude from 50 km in the south to as little as 10 km in the north (Stewart, 1967; McKee, 1968; Snow and Wernicke, 1989), and became active 15 Ma.

Structurally connected to the FLVFZ to the east, the Emigrant Peak Fault Zone (EPFZ) (Reheis and Sawyer, 1997) serves as the range front fault of the northern SPR (Fig. 1.1) and is geometrically analogous to other systems in the region including faults which bound RSM further north within the Mina deflection (Ferranti, 20090. The curved surface expression of the EPFZ is comprised of normal faults down to the west, which cut Pliocene to Quaternary alluvial and lacustrine deposits (Reheis, 1991; Reheis and Sawyer, 1997). The westernmost strand of the fault zone trends east-northeast for approximately 8 km in its southwestern exposure, and then turns north-northeast for approximately 18 km where it appears to intersect east-northeast trending faults in the northern part of the SPR. The curved surface expression of the EPFZ is comprised of normal faults down to the west which cut Pliocene to Quaternary alluvial and lacustrine deposits (Reheis, 1991; Reheis and Sawyer, 1997).

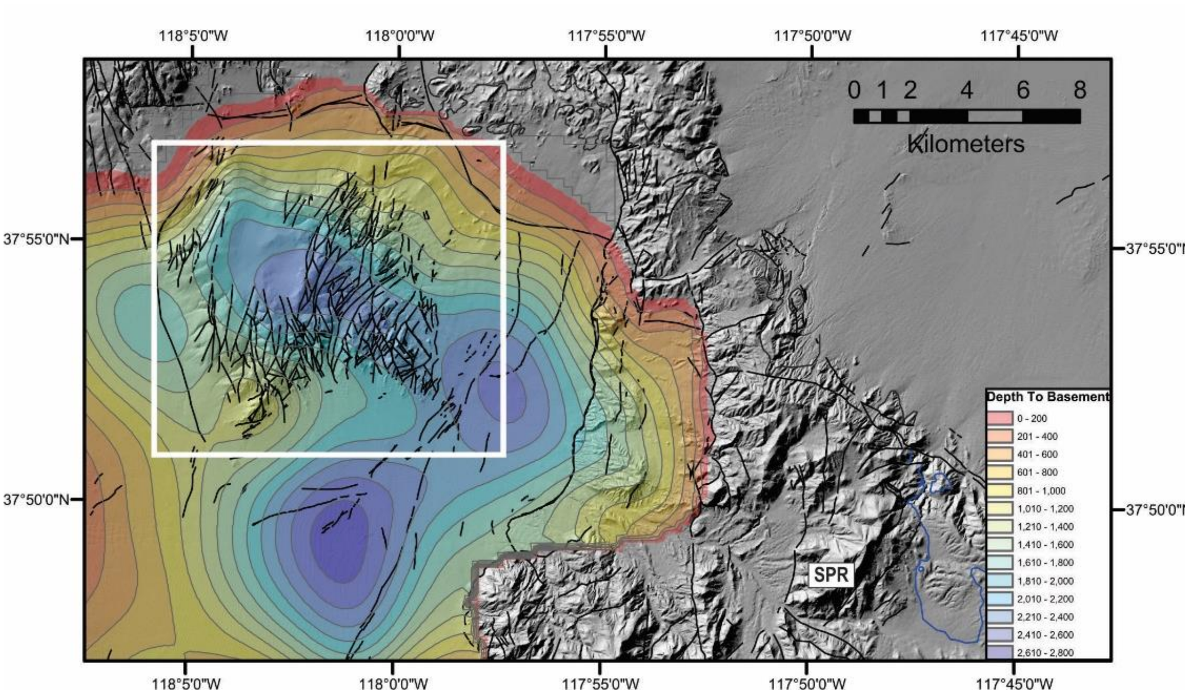

Figure 2.1. 3-D depth inversion of northern Fish Lake Valley superposed on the fault geometry showing localized sub-basins ranging from 1.8 km to 2.8 km. The basin in the center of the SVH opened at ~ 13 Ma as a result of movement on the detachment in the SPR. To the east of SVH, an ~2.6 km deep basin developed from down to the west displacement on the EPFZ. The RCBA was inverted for depth in 3-D by Nicholas Mueller.

Within the hanging wall of the curved EPFZ, (Fig. 2.1) the SVH, which is bound by a curvilinear range front fault, is geographically separated from the SPR by a 2.6 km deep basin (Mueller et al., 2016). The deposition of volcanic rocks and the fault geometry of the SVH is directly controlled by down to the west movement of structures in the SPR. The faults located within the SVH are an array of east-northeast, north-northwest and northeast trending high-angle faults which record the progressive complex kinematics during movement on the SPLM low angle detachment followed by displacement on the EPFZ during basin evolution (Ng, 2017). Volcanic and sedimentary rocks of the SVH include three members of a succession known as the Coyote Hole Group and in stratigraphic order from oldest to youngest are; Silver Peak Formation, Rhyolite Ridge tuff, and Argentite Canyon Formation. The volcanic and sedimentary succession ranges in age from 13-5 Ma and consists of tuffaceous sediments, welded to non-welded ash-flow tuff, and lava. Unconformably overlying the Coyote Hole Group, Fish Lake Valley assemblage is a group of interbedded lacustrine sediments, basalt, and basaltic andesitic flows dated at 4-5 Ma. Volcanic and sedimentary rocks in the SVH were deposited in localized basins active during displacement on the SPLM detachment followed by movement on the EPFZ.

CHAPTER 3

GEOLOGY OF THE SOUTHEASTERN VOLCANIC HILLS

The Tertiary stratigraphy of the SVH records a complex history of sedimentary succession that includes two of the three late Cenozoic units recognized in the SPR by Oldow et. al (2009) and in surrounding mountain ranges. These include three unconformably bounded members of the Coyote Hole Group; Silver Peak Formation, Rhyolite Ridge tuff, and Argentite Canyon Formation (Cave Springs Formation is absent in the SVH), in ascending stratigraphic order. Rocks comprising the SVH have a broad range of compositions ranging from siliceous tuff, to basaltic lava, and sedimentary units consisting of fine- to coarse-grained siliciclastic rocks. Unconformably overlying the Coyote Hole Group, Fish Lake Valley assemblage is composed of lacustrine sediments, basalt, and basaltic andesitic flows dated at 4-5 Ma. The stratigraphy exposed in the SVH is geographically restricted and form distinct domains: western (Silver Peak Formation), central (Rhyolite Ridge tuff and Argentite Canyon Formation), and eastern (Fish Lake Valley assemblage) domains. In the SVH abrupt thickness variations of the Tertiary stratigraphy occur across a complex system of faults active from the Miocene to present day.

The high-angle faults in the SVH form a system of structures oriented north-northeast to northeast and northwest to north-northwest and were active during the deposition of late Cenozoic volcanic and sedimentary rocks. The timing between fault activity and deposition can be discerned through analysis of detailed stratigraphic relationships, and will be analyzed later in the paper, by modeling growth relations in members of the Coyote Hole Group, specifically Rhyolite Ridge tuff. High-angle faults in the SVH have a complex geometry with mutually cross-cutting relationships between north-northwest and north-northeast structures (Fig. 3.1). However, some northwest striking faults were subsequently sealed by the overlying Argentite Canyon Formation (Fig. 3.2). High-angle faults in the SVH are controlled by the basin

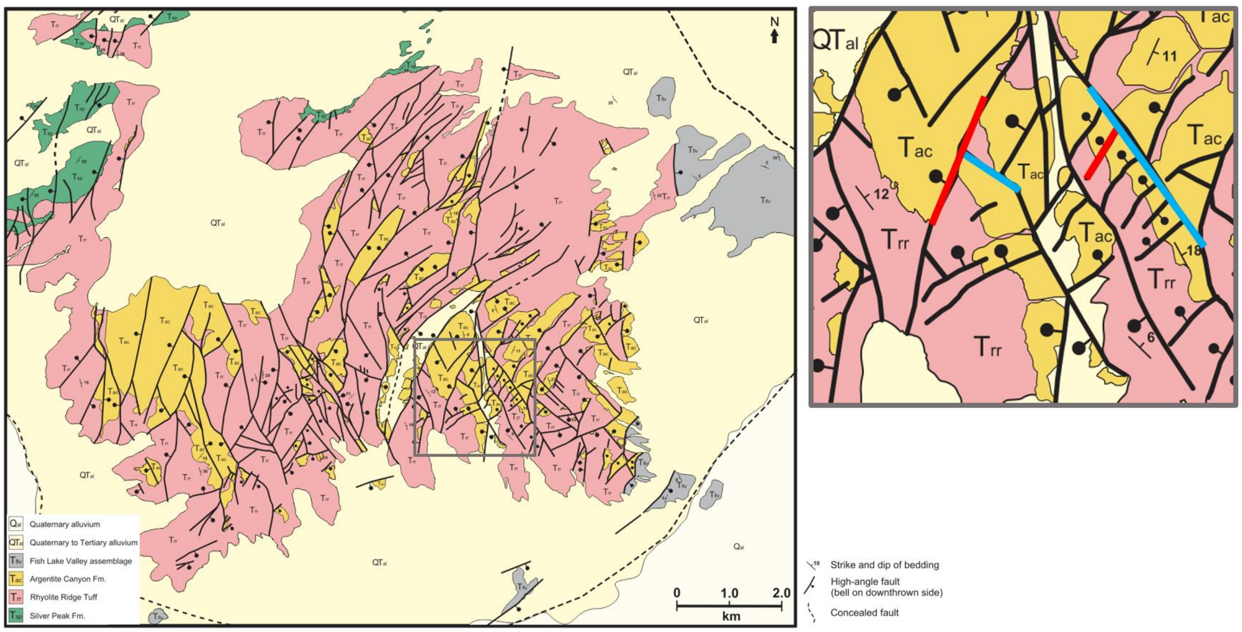

Figure 3.1. Geologic map of the SVH with an outlined box in gray increased in size to the right of map showing mutually cross-cutting fault orientations between north-northeast to northeast striking faults (blue bold lines) and north-northwest striking faults (red bold lines).

bounding structures that surround the area in two generations of faulting. The first generation was controlled by high-angle faults which soled into the westward translating movement on the SPLM detachment fault during the Miocene, whereas, the second generation is controlled by westward movement of the curved EPFZ which cut the detachment system at approximately 5 Ma.

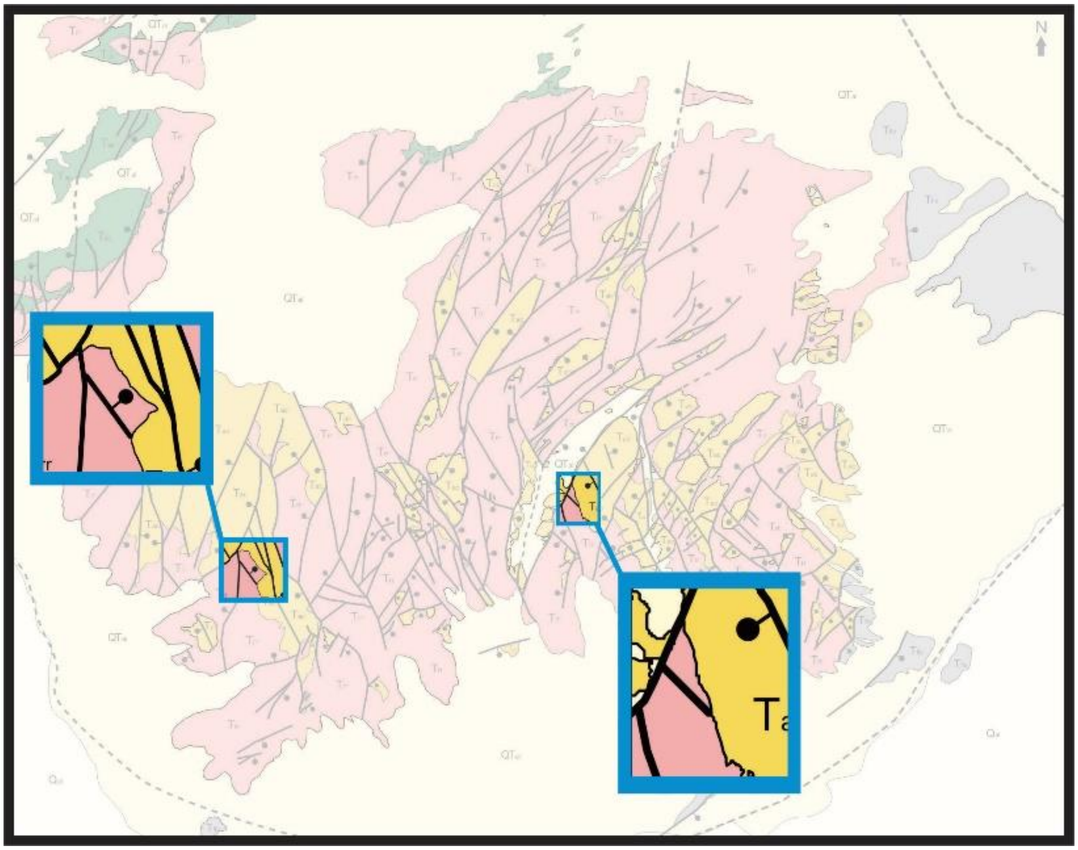

Figure 3.2. Geologic map of the SVH with highlighted location where north-northeast striking faults cutting Rhyolite Ridge tuff are overlain and sealed by Argentite Canyon tuff.

3.1 Coyote Hole Group

This older late Tertiary volcanogenic-volcanic succession exposed in the southeastern Volcanic Hills is crucial to determining the progressive deformation associated with large magnitude extension during movement on both the SPLM detachment system followed by the initiation of the EPFZ. The members of the Coyote Hole Group have lithologically distinct, and in particular variation in thickness of each member in SVH reflect changes in the direction and magnitude of extension in the study area. Two units show a substantial difference in thickness across fault strike, observed on well-exposed depositional contacts which were measured across the structural contacts. Well log data in the SVH, exhibits a similar patterns of increased thickness in members of the Coyote Hole Group, which was also noted by Oldow et al. (2009) in the Silver Peak Range, to the east across the Fish Lake Valley basin. Rocks of the Coyote Hole Group are explained in detail in successive stratigraphic order in the following sections.

3.1.1 *Silver Peak Formation*

In the southeastern Volcanic Hills, outcrops of the basal unit of the Coyote Hole Group, Silver Peak Formation, are geographically restricted to the north and northwestern extent of the study area (Tsp Fig. 3.1). In the northwest portion of the SVH, a canyon exposes approximately 100 meters of interbedded tuff and tuffaceous sediment. The same upper member of the Silver Peak Formation can be correlated in the north of the mapping area, but the basal section seen in the canyon is obscured by Quaternary and Tertiary alluvium. In the SVH, the SPF is overlain unconformably by Rhyolite Ridge tuff, but is not found in contact with the underlying stratigraphy. However, in the Silver Peak Range, the SPF is documented to rest depositionally on the Tertiary Ice House Canyon assemblage as well as Paleozoic rocks and is found in structural contact with metamorphic tectonites associated with the lower plate of the SPLM extensional complex (Oldow et. al, 2009). Although the base of the Silver Peak Formation is not exposed in the SVH, bore hole data (Fig. 3.3) provides constraints for thickness variations and gives evidence the formation rest depositional on the Tertiary Ice House Canyon assemblage and Paleozoic rocks (Fig. 3.3, well 88-11).

In the study area, the Silver Peak Formation thins from southwest to northeast, with thickness from interpreted and correlated well logs in the northern FLV decreasing from 380-850 m in the south to 30 m in the northeast (Fig. 3.3). The SPF consists of interbedded shale, tuffaceous sandstone, and conglomerates containing Tertiary volcanic and Paleozoic clasts in this area, and exposed sections range from 1 to 10 m thick, displaying prominent cross-bedding in the

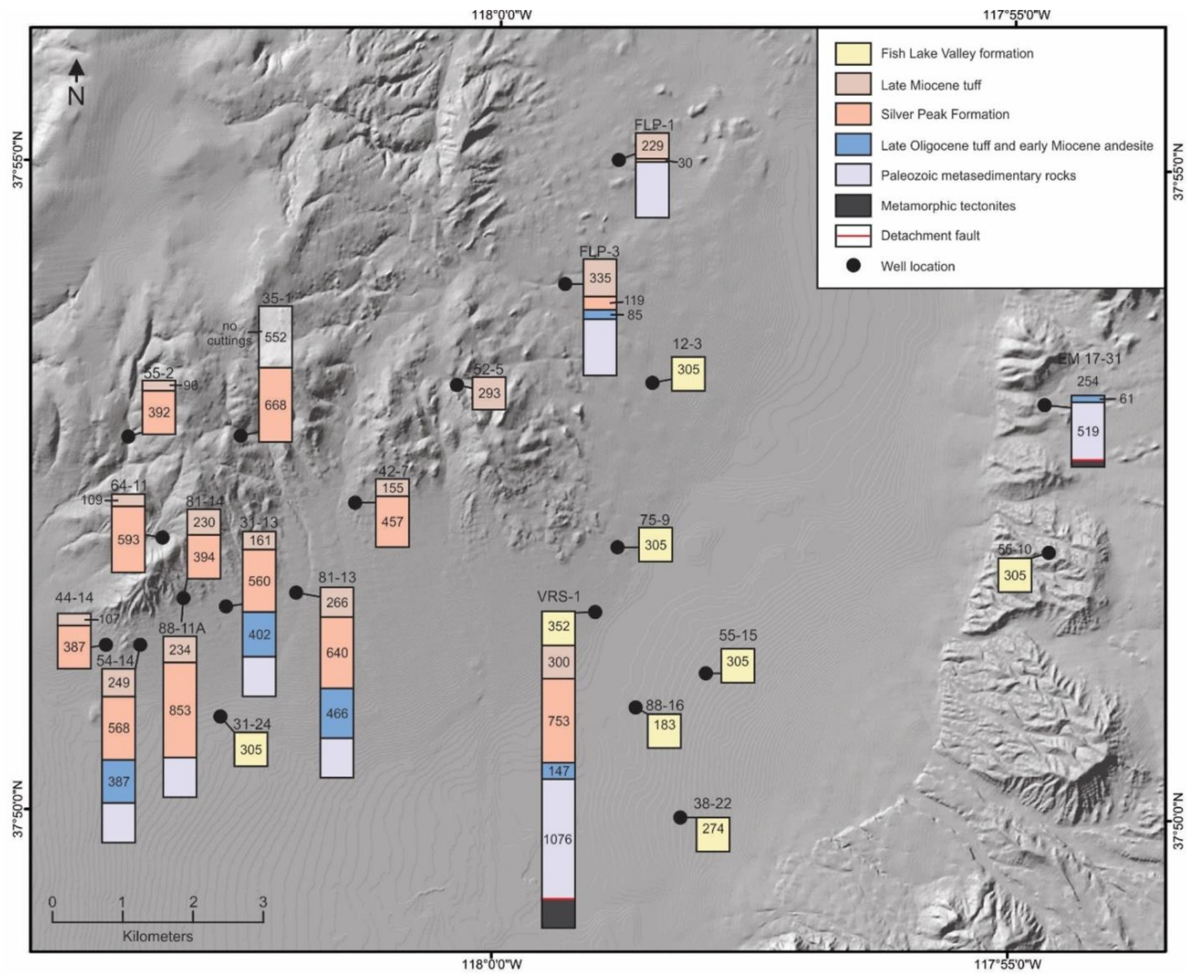

Figure 3.3. Interpreted stratigraphic sections of well lithologic logs in northern Fish Lake Valley (taken from Oldow 2016). Numbers are thickness of each unit in meters.

tuffaceous sandstone. K-Ar dating of the Silver Peak Formation was conducted on interbedded tuffs, and revealed an age of 11-13 Ma (Stewart and Diamond, 1990; original dates reported by: Everden et al., 1964; Everden and James, 1964; McKee and Glock, 1984). In the northwestern

SVH where Silver Peak Formation outcrops samples of vertebrate and plant fossils yield a similar middle Miocene age (Robinson et al., 1968).

3.1.2 *Rhyolite Ridge Tuff*

Exposures of Rhyolite Ridge tuff dominate in the central portion of the mapping area and are in contact with all lithologic units mapped in the SVH (Fig. 3.4), including; Silver Peak Formation, Argentite Canyon Formation, and Fish Lake Valley assemblage. The volcanic rocks of Rhyolite Ridge tuff overlie Silver Peak Formation with an angular discordance in the western SVH. Although the basal unit of Rhyolite Ridge tuff appears at the surface throughout the region, it is only exposed in contact with Silver Peak Formation in the northwestern and northern portions of the mapping area. Similar angular discordance between the two units is likely in the eastern and southern portion of the SVH as well.

The Rhyolite Ridge tuff is dated at 6.148 ± 0.019 Ma (Oldow, 2009) to the south of the Silver Peak Range, and beneath the upper contact of the tuff with the overlying Argentite Canyon Formation a sample yielded a $^{40}Ar/^{39}Ar$ age on sanidine of 6.03 ± 0.03 Ma (Oldow, 2009). The Rhyolite Ridge tuff in the study area was divided into five distinct members that are lithologicaly similar but differ in color, percentages of phenocryst, lithics, and matrix, as well as the degree of welding. The basal unit (Trr1) is a non-welded ash flow tuff which contains 10 to 20 percent lithic and pumice clasts, in a matrix composed of 25 to 50 percent phenocrysts of sanidine (70%), biotite (5%), and quartz (25%) supported in an ash matrix. Phenocryst size and crystal habit differs with sanidine and biotite ranging from subhedral to euhedral and 1 to 2 mm, and quartz is 1 mm in diameter. Lithic fragments make up between 10 to 20 percent of the tuff and are equally divided between rock fragments and pumice. Lithic clasts are sub- rounded to subangular, ranging from 1 to 8 cm, and composed of weathered rhyolite lava. Trr2 is a weakly welded ash flow tuff which contains 60 to 70 percent lithic and pumice clasts, in a matrix composed of 25 to 50 percent phenocrysts of sanidine (70%), biotite (10%), and quartz (20%) supported in an ash matrix. Phenocryst size and crystal habit are identical to Trr1. The majority of lithic clast are pumice and range in size from 1-8 cm. Trr3 is the most distinct member of Rhyolite Ridge tuff and can easily be traced as a marker bed across the mapping area. The member is a non welded ash flow tuff, in a matrix composed of 30 percent phenocrysts, made up of sanidine (70%), biotite (5%), and quartz (25%) supported in a light gray ash matrix. The most distinguishable aspect of Trr3 are 1-5 cm rounded clasts of obsidian which make up 10- 20 percent of the member ("Apache tears"). Trr4 is a moderately welded ash flow tuff which contains 10 percent lithic fragments. Very few pumice clasts are present, and the matrix is composed of 60 percent phenocrysts comprising sanidine (60%), biotite (10%), and quartz (20%). Sanidine phenocryst are subhedral to euhedral and 1 to 2 mm, and quartz 2 mm in diameter. Lithic fragments make up between 10 to 15% percent of the tuff and are sub-angular, ranging from 1 to 2 cm. The upper most member Trr5, is a moderately welded tuff composed of 20 to 30 percent lithic and pumice clasts, in a matrix composed of 25 to 50 percent phenocrysts of sanidine (70%), biotite (5%), and quartz (25%) supported in an ash matrix. Phenocryst size and crystal habit differs with sanidine and biotite ranging from subhedral to euhedral and 1 to 3 mm, and quartz 1 mm in diameter. Lithic clasts make up between 10 to 20 percent of the tuff and are equally divided between lithic fragments and pumice. Lithic clasts are weathered rhyolite lava, sub-rounded to sub-angular, ranging from 1 to 3 cm. In areas where the Argentite Canyon

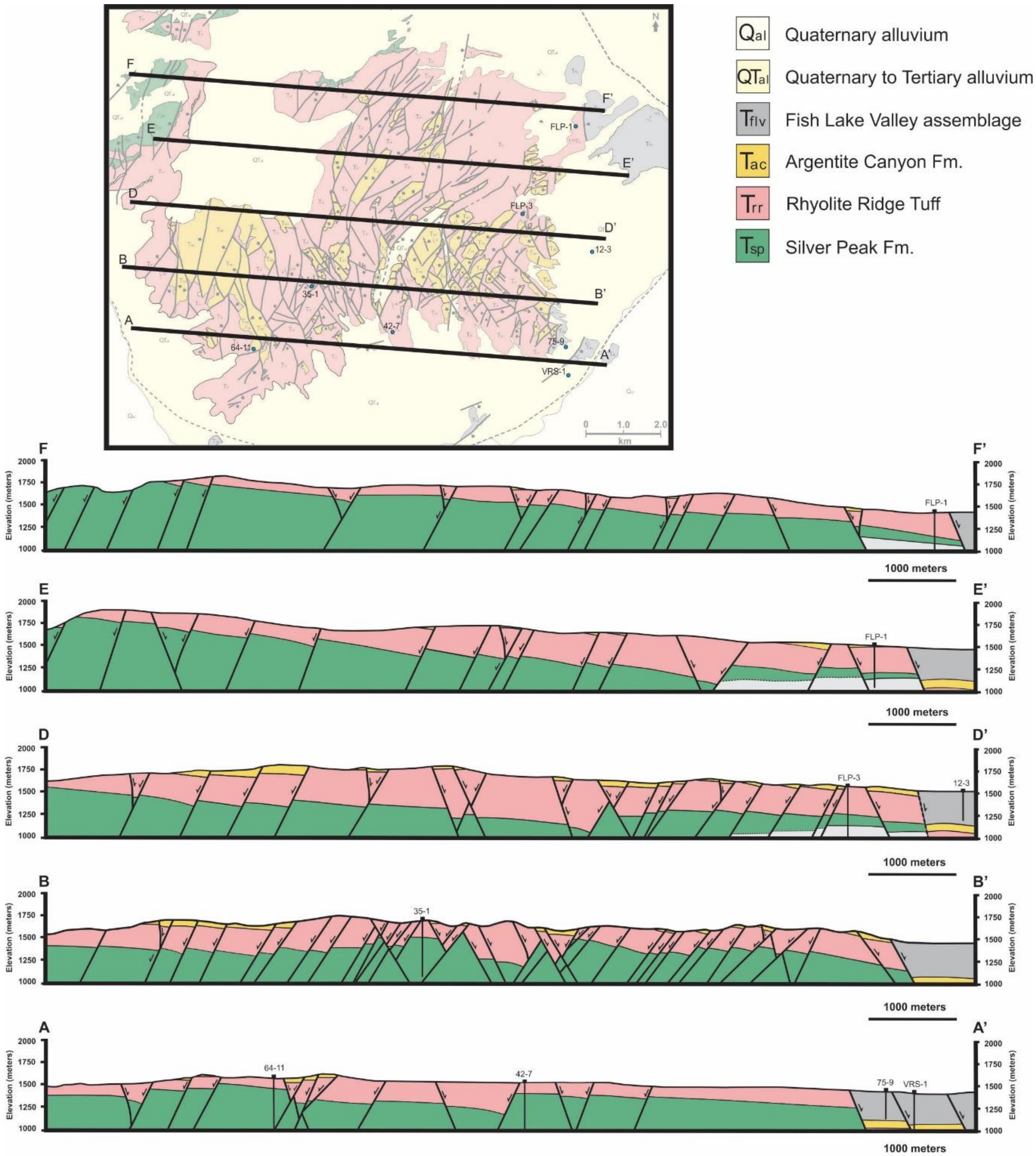

Figure 3.4. Cross sections showing unit thickness variation and the distribution of high-angle faults in the southeastern Volcanic Hills. Fault dips are typically 50-80° where mapped. Approximate unit thicknesses are constrained from well logs (Fig. 3.3) and surficial geology (Fig. 3.1).

Formation exhibits a vitrophyre and rests on Trr5, Trr5 has been altered ("baked") to a gray-pink vesicular glass. The members Trr1-5 are traceable throughout the mapping area but in the north and some portions of the south are too heavily altered to distinguish from each other.

Relative thicknesses of the Rhyolite Ridge members varies with structural setting in the field area (Fig. 3.5). From the cross section, the members of Rhyolite Ridge tuff demonstrates an abrupt increase in thickness from 200 m to 600 m over a single north-northeast striking down to the west fault (Fig. 3.5, C-C', bolded black fault). The members continue to gradually thin toward the western extent of the area, but remain thicker than to the east where they reach a maximum of approximately 300 meters.

3.1.3 Argentite Canyon Formation

Argentite Canyon Formation is the upper unit of the Coyote Hole Group and lies in unconformable contact with Rhyolite Ridge tuff throughout the SVH. Argentite Canyon Formation occurs sparsely throughout the mapping area and there is no indication of major thickness variations. The upper contact of Argentite Canyon Formation is erosional and as a consequence formation thickness and its relation to displacement on faults is indeterminate. The greatest preserved thickness is 75 m in the eastern portion of the mapping area, where it is in structural contact with the overlying Fish Lake Valley assemblage. To the east across, Fish Lake Valley Basin, in the Silver Peak Range outcrops of the formation reappear in synextensional sub-basins (Oldow, 2009).

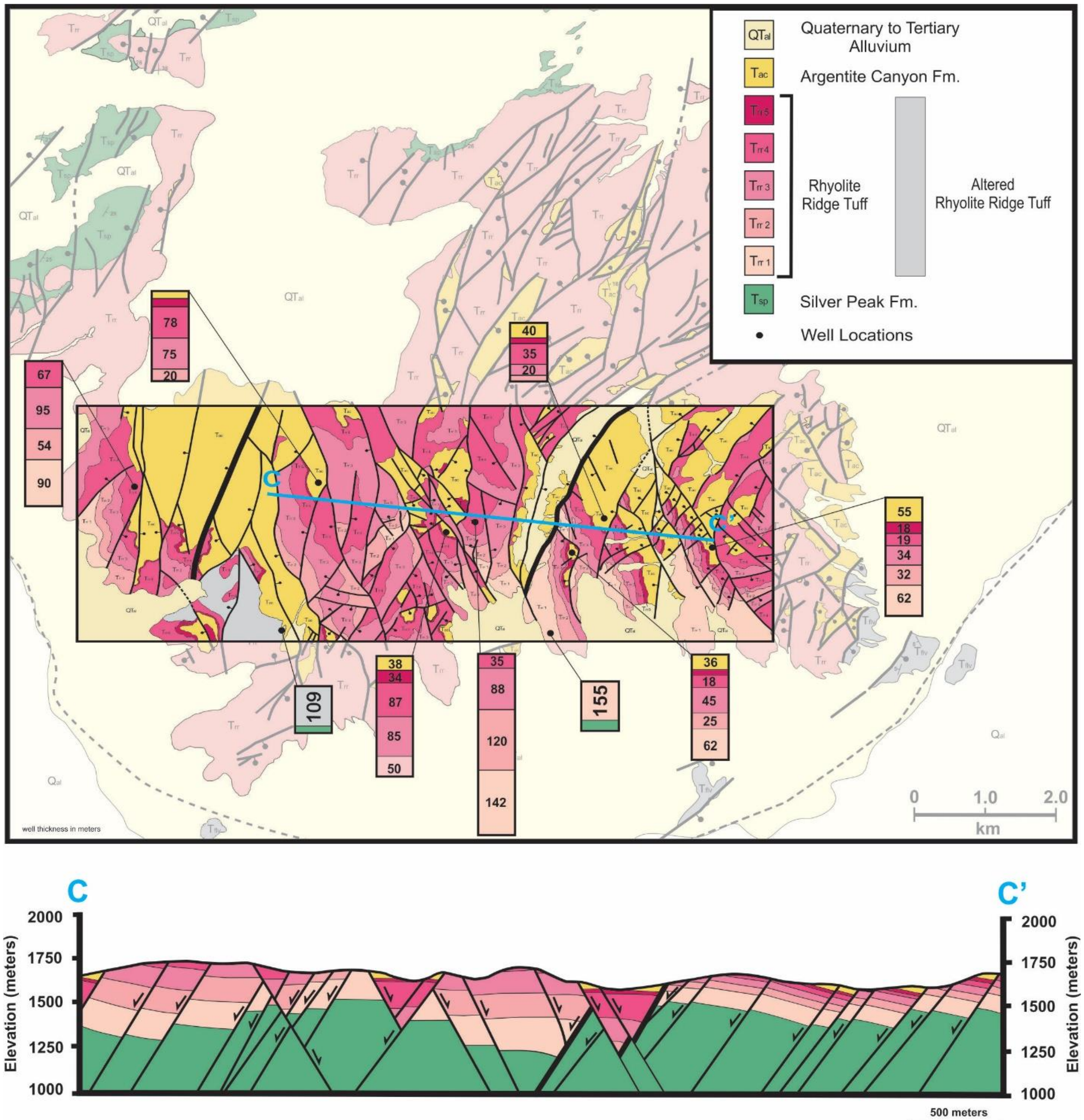

Figure 3.5. Geologic map with field-measured (horizontal label) and well log interpreted (vertical label) thickness of the five Rhyolite Ridge members defined for the field area. Observed thickness variation of Rhyolite Ridge tuff due to synextensional deposition accommodated by high-angle faults during movement on the low-angle SPLM detachment faults.

Argentite Canyon Formation in the SVH is composed predominantly of erosional remnants of welded, porphyritic ash-flow tuff, generally marked by a 10 m thick basal vitrophyre occasionally weathered to a fine grained gray to black very fine sand to silt size particles. The signature vitrophyre at the base of Argentite Canyon Formation is not laterally continuous and generally absent in the northern part of the mapping area, making the contact between Rhyolite Ridge tuff and Argentite Canyon Formation ambiguous in that area. Robinson et al. (1976) reported K-Ar ages of 5.9 and 6.1 Ma flows exposed to the east of Fish Lake Valley Basin where Cenozoic outcrops are overlain by rocks of the Fish Lake Valley assemblage. Oldow et. al (2009) provided $^{40}Ar/^{39}Ar$ dating on sanidine in two locations, one at the base of the unit where it lies unconformably on Rhyolite Ridge tuff, and another sample from the top where Argentite Canyon Formation is overlain by Fish Lake Valley assemblage. The samples yielded an age of 5.87 ± 0.02 Ma and 5.85 ± 0.03 Ma, respectively.

3.2 Fish Lake Valley Assemblage

The Fish Lake Valley assemblage unconformably overlies Argentite Canyon Formation in the eastern most extent of the SVH, but in some areas is in structural contact with Argentite Canyon Formation and the Rhyolite Ridge tuff where the bounding faults that control the northern FLV basin drop down to the east (left side of white boxed area, Fig. 2.1). Fish Lake Valley assemblage is geographically limited to topographically low areas in the southern and eastern extent of the mapping area (Fig. 3.6). Basin bounding high-angle faults in the eastern portion of the SVH, and contemporary down-to-the-west movement of the EPFZ created

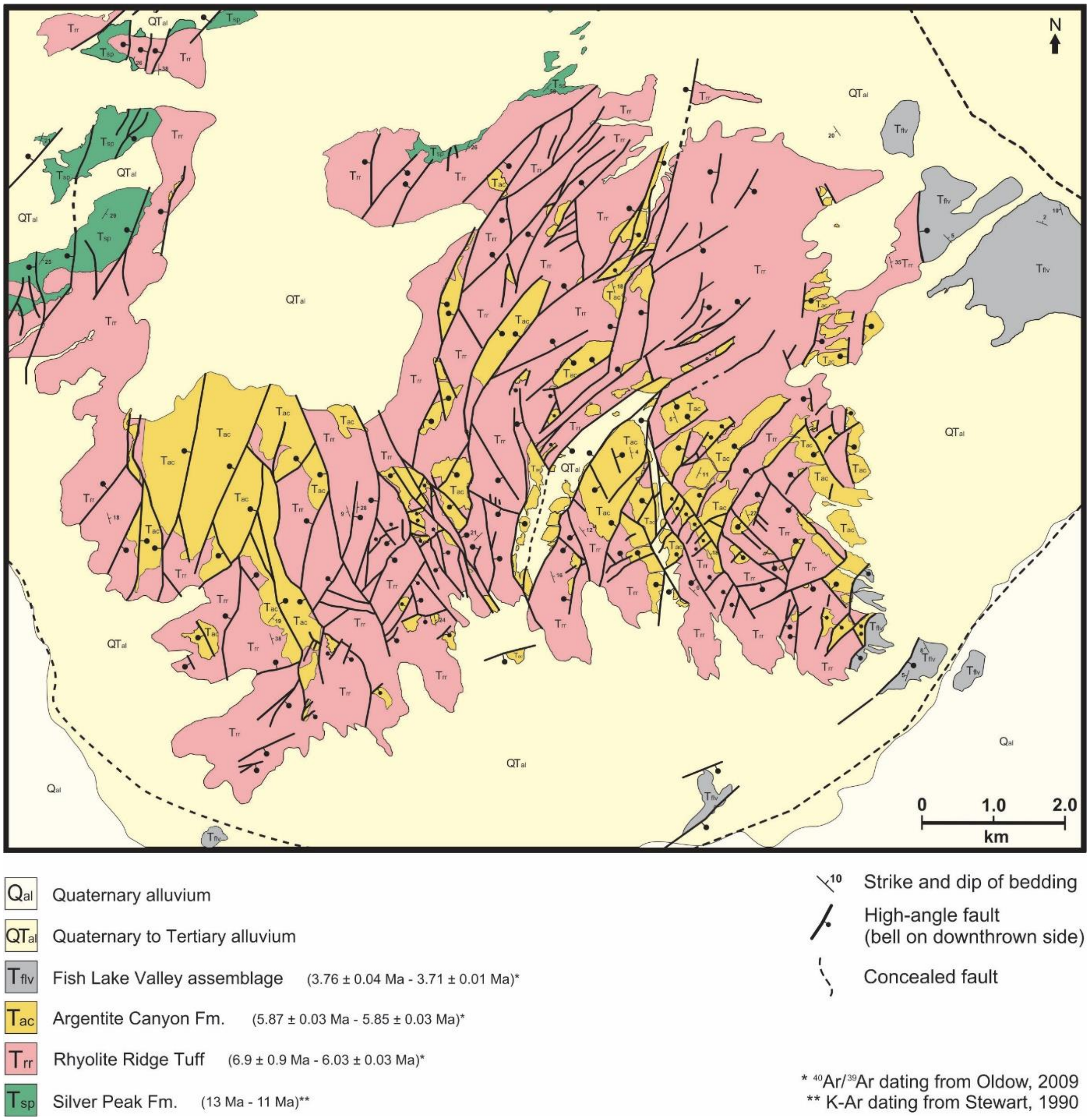

Figure 3.6. Geologic map of the southeastern Volcanic Hills showing the distribution of lithologic units and their surficial geographic locations.

accommodation space for the deposition of Fish Lake Valley assemblage. Borehole data, analyzed by Reheis et al., (1993), and integrated with surficial geologic evidence provide critical constraints in determining subsurface geology and thickness variations of Fish Lake Valley assemblage (Fig. 3.4). West of the basin bounding faults, the Fish Lake Valley assemblage, exhibits a roughly constant thickness of 300-350 m (Fig. 3.3) from north to south. In the eastern extent of SVH, to the east of those faults, in the central portion of FLV basin, the assemblage has been modeled in gravity studies to be up to 1.1 km thick (Ng, 2017). Exposed sections of the Fish Lake Valley assemblage on the eastern flank of the SVH are composed of a basal conglomerate overlain by interbedded sections of coarse grained sandstone, fine grained sandstone, and laminated mudstone. In some areas green to brown argillite layers are found interbedded in the upper sections, but are not laterally continuous. A single basalt flow outcrops in the pediment of the southwest portion of the SVH and is the only basalt exposure in the mapping area. Near the western flank of the central SPR, basalt flows exposed near the base of the section found whole-rock $^{40}Ar/^{39}Ar$ ages of 3.71 ± 0.01 and 3.76 ± 0.04 (Oldow et. al, 2009).

CHAPTER 4

FAULT GEOMETRY OF THE SOUTHEASTERN VOLCANIC HILLS

The Tertiary structures of the SVH are complex and reflect the progressive disarticulation and extensional history of upper plate volcanic rocks as movement on the SPLM detachment occurred and then subsequently as the EPFZ opened the eastern most basin in northern FLV. Details of the timing and magnitude of these movements are revealed by syn-tectonic thickness changes in the Coyote Hole group (discussed above), and fault orientation and cross-cutting relationships discussed below. Within the western SVH high-angle faults predominantly strike northwest to north-northwest and north-northeast and some are traced with confidence up to 5 km in length before being covered by quaternary alluvium to the north (Fig. 2.1 and Fig. 3.4). North-northeast structures and north-northwest structures are found merging in some areas, as well as mutually cross-cutting one another in other areas (Fig. 3.1). In the eastern SVH there are two sets of dominant structures, the most important of which is a curvilinear system of faults that can be traced up to 6 km and is oriented from north-northeast in the south turning northeast in the northern SVH (Fig. 3.6). The thickness of Miocene volcanic rocks varies substantially across the main curved faults (bolded black lines, Fig. 3.5). Some north-northeast striking faults do not curve and continue almost due north into the western SPR. The second orientation of structures strike north-northwest to northwest and are generally only traceable for moderate distances (1500 meters). The relationship between the north-northeast to northeast structures with the north-northwest to northwest structures is mutually cross-cutting (Fig. 3.1) with a slight preference of the northeastern faults being younger than northwest striking structures in the south, but in the north the opposite relative age relationship is found. At the southern edge of the mapping area, structures tend to be parallel to the basin bounding fault (east-northeast), but are imperfectly exposed due to pediment cover. In two locations in the west and central areas, north-northwest fault segments cut Rhyolite Ridge tuff and are later sealed by Argentite Canyon Formation (Fig. 3.2).

CHAPTER 5

FAULT-SLIP INVERSION

Temporal and spatial evolution of strain in the SVH can be evaluated through the application of fault slip inversion. Indeed, four distinct generations of extension can be recognized for the SVH using this method. Analysis and the kinematic history of displacement in the SVH is given by the assessment of over 350 in field measurements of slickenside lineations with shear-sense indicator determinations. At least three, but typically more, non-parallel striated faults were used for assessing a specific kinematic episode at any one location (e.g., Bellier and Zoback, 1995). Measurements are concentrated in Cenozoic volcanic and sedimentary rocks on variable orientations of high-angle faults and in the damage zones of major faults in the mapping area (~1560 km2). For the determination of slip direction on the fault plane a detailed interpretation of shear sense criteria (Reidel shears) linked to secondary fractures which form in response to stress and strain conditions present at the time of displacement was analyzed (Petit, 1987). Mineral fibers and tool marks were observed and provided a secondary verification of the sense of slip. In field data were plotted first by hand using a Schmidt equal-area lower hemisphere stereographic projection and then graphically plotted using Fault Kin 7 stereonet program (Allmendinger et al., 2012) to invert the fault-slip datum for incremental strain axes orientations. The use of fault slip inversion for describing strain conditions operating in the Walker Lane is supported by earthquake focal mechanism and GPS velocity fields (Ryall and Priestley, 1975; Zoback, 1989; Rogers et. al, 1991; Oldow, 2003).

In the SVH, the segregation of data was critical to determining the number of distinct kinematic events and relative timing of those episodes due to the slip data measurements being in virtually every orientation (Fig. 5.1 a). Fault slip measurements were separated into kinematically distinct groups for further analysis using the principles of strain compatibility discussed by Angelier et al. (1984) and Marrett and Allmendinger (1990). Criteria for differentiating incompatible movement on parallel fault planes includes; measurements with an opposite shear sense indicators, orthogonal sense of slip, and a variance of greater than 20° in the angle between slickenside lineations (Merrett and Allmendinger, 1990). The relative timing of separate deformation events were determined by direct observation of cross-cutting slickenline measurements on the fault surface together with back stripping data which belongs to the youngest known extension first (west-northwest). In the following paragraph detailed examples of data from the SVH are explored which illustrates four separate extension directions.

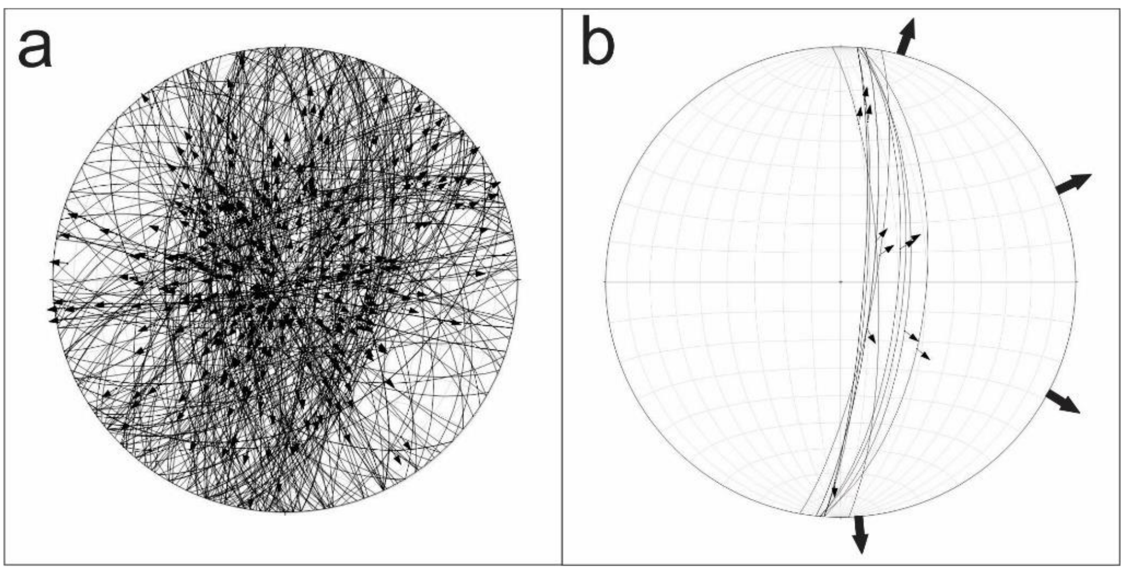

Figure 5.1. Stereonets showing orientations of fault planes and sense of slip. Figure a. represents all the data collected in the SVH. Figure b. represents four incompatible extensional orientations on faults oriented from 0-10 degrees.

The measurements in Fig. 5.1 b, show similar oriented planes with opposite shear sense indicators or orthogonal sense of slip and infers distinct kinematic events or fault reactivation.

The eight subparallel fault planes (0-10 degrees), show four different directions of extension (north-northeast, east-northeast, west-northwest and north northwest) with four distinct

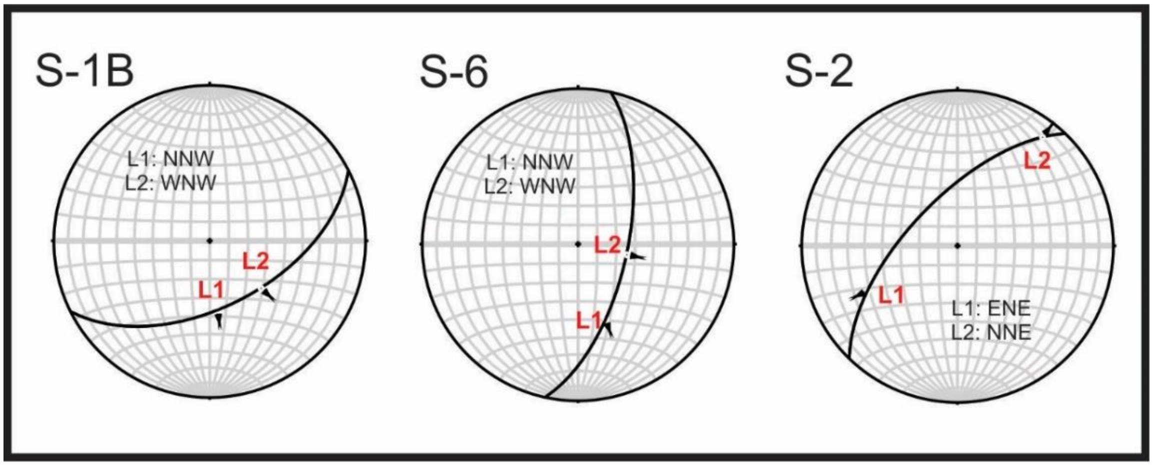

Figure 5.2. Stereonet data demonstrating incompatible slip orientations on a single fault plane.

shear sense indictors orientations; left lateral, left oblique, right oblique, and right lateral, respectively. Merrett and Allmendinger (1990) note that slickenside lineations with a variance of greater than 20° may indicate fault reactivation has occurred. However, this number should be used with caution since faults with a greater incline to the extension direction will have a fuller range of slip possibilities, (Angelier, 1984; Zoback, 1989). We use superposition of slip data to verify if multiple events of extension have occurred or if we are observing a scatter in slip. It is common for measurements to be non-unique and possibly grouped in to multiple extension directions, in which case the data was grouped in the most modern extension direction (west-northwest) with the same kinematic compatibility unless super positioning was able to verify different. In Fig. 5.2, two superposition measurements were taken on variably oriented fault planes. S-6 shows a north-northeast trending fault with two superposed measurements, L1 has a right-oblique sense of movement and L2 is purely dip-slip. Although it is possible for movement to occur both with a right oblique and normal slip on the same fault plane, in the same extension, the spread of data indicates two separate events, north-northwest and west-northwest. S-1B fault plane is oriented west-northwest and also has two superposed slickenline measurements. However, in this case opposite directions of shear sense were observed, L1 (north-northwest extending) right-oblique movement and L2 (west-northwest extending) left oblique movement. Faults moving in opposite directions on the same plane are not compatible and further verifies movement in two separate events. Similar superposition relationships can be seen in Fig. 5.2, stereonet S-2, which shows opposite shear sense indicators, L1 (east-northeast extending) moving left oblique and L2 (north-northeast extending) moving right-lateral suggesting two separate extensional events have imprinted on the same fault plane, an east-northeast and north-northeast extension, respectively. The process of determining different kinematic families is an iterative process which requires all components of compatibility together with the analysis of superposed lineations to be attentively segregated so a full picture of the movement history can be realized. Striae relations indicate four generations of extension are present in the SVH; N68°W, N21°E, N70°E, and N23°W. The orientation of strain axes was estimated to within five degrees, and assign a ±10° uncertainty to the determined direction of extension based on the average difference in degree of slip between kinematically homogeneous measurements.

Faults that accommodate movement associated with the four different kinematically homogeneous extensional events range in orientation and the sense of slip systematically varies as the fault orientation changes (Fig. 5.3). Faults grouped in the west-northwest extensional

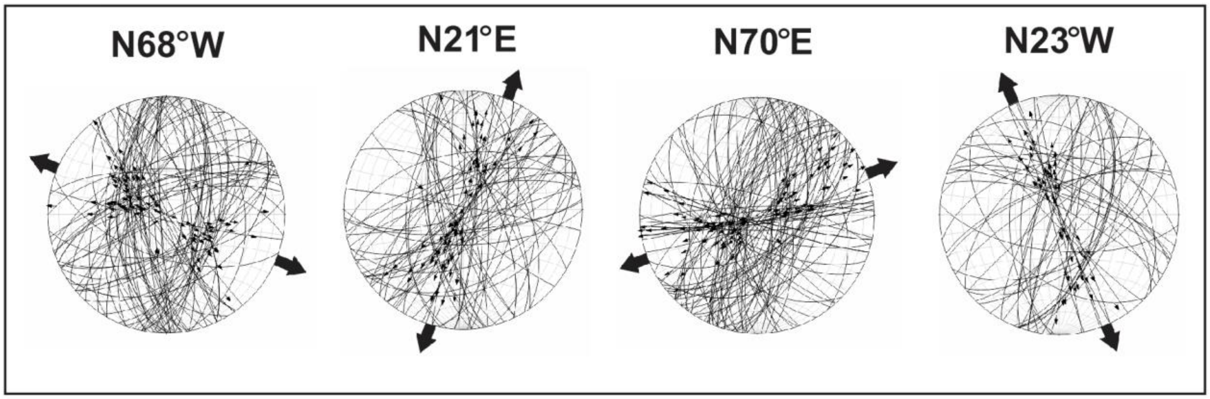

Figure 5.3. Stereographic projections of the extension direction in the SVH.

event have fault orientations ranging from northwest to east-northeast. The most common orientation in the west-northwest kinematic family of faults are north-northwest striking faults which have a right-oblique sense of slip and dips of 60 degrees to nearly vertical. Northeast to east-northeast striking faults are left-oblique to left-lateral respectively and dip 30-85 degrees, with the gentler dips having a left-lateral sense of motion. Northwest striking faults are right-oblique to right lateral. North-northeast extending fault slip measurement are inverted from west-northwest extending faults. North-northwest striking faults are left-oblique to left-lateral and northeast to east-northeast oriented faults move in right-oblique to right-lateral direction. Reversal of fault motion only occurs once and is on the less common northwest oriented fault planes. East-northeast extending faults move almost purely dip slip with a minor right oblique movement on north-northwest to northwest striking faults and left oblique to left lateral on north-northeast to northeast oriented faults. Whereas, north-northwest extending fault slip datum have left-oblique to left-lateral slip on west-northwest to northwest trending faults and right-oblique to right-lateral slip on north-northwest to north-northeast striking faults.

5.1 Slip History

The nature of cross-cutting relationships between faults is the most straightforward way to evaluate strain evolution in SVH; alas the analysis is complicated by the presence of mutually cross-cutting slip direction indicators. Careful analysis indicates an earlier period of east-northeast and north-northwest mutually cross-cutting slickenlines was followed by a superposed period of west-northwest and north-northeast mutually cross-cutting slip lineations. In Fig. 5.4, the complicated relationship is graphically demonstrated between the four different strain fields by superposed slip lineations observed in the field. At sites S-7, S-1, S-3 and S1-B, S-5, S-6, west-northwest slickenside lineations are superposed on east-northeast and north-northwest lineations respectively. In stereonets S-1 and S-3 northwest striking faults dipping south bare left lateral east-northeast extending first generation movement (L1) superposed by a dip-slip to left-oblique west-northwest movement (L2). Stereonet S-7 is a north-northwest striking fault with left oblique east-northeast first movement followed by right-oblique slip extending west-northwest. S1-B strikes east-northeast and displays a right-oblique north-northwest extending first movement superposed by a left-oblique west-northwest extending movement. Locations S-5 and S-6 both strike north-northeast, and dip steeply to the southeast and display west-northwest extending fault-slip measurements superposed on north-northwest extending striae. In stereonet S-5 the west-northwest measurement is slightly more oblique than S-6 and could be due to movement of the fault block or the fault plane having a slightly lower angle dip to the extension direction. At sites S-4 and S-2 north-northeast extending lineations are superposed over north-northwest and east-northeast oriented slickenside surfaces. S-4 first movement (L1) is north-northeast extending right-lateral motion, whereas the second movement (L2) is a left-lateral north-northeast extending movement. At no locations was the inverted relationship found, west-northwest extension (light blue) always superposes east-northeast (dark blue) and north-northwest (orange) directed extension, and north-northeast extending striae (yellow) always superposes north-northwest (orange) and east-northeast (dark blue) movement vectors. From the relationship outlined above, we can deduce relative timing between two phases of superposed motions (Fig. 5.5). The first phase has east-northeast and north-northwest directed movement, and the second phase has west-northwest and north-northeast extending movement.

5.1.1 Phase Two – Mutually Cross-cutting West-northwest and North-northeast Slip Lineations

Fault-slip analysis in the SVH demonstrates mutually cross-cutting relationships between west-northwest and north-northeast slip lineations. The complicated relation between the two strain fields is illustrated by slip lineation superposition observed at several sites in the SVH. Phase two mutually cross-cutting slip lineations were documented in seven locations in the SVH (Fig. 5.6), four of the locations (D2-1, D2-2, D2-4a, D2-6c) have a slip lineation relationships displaying north-northeast slip superposed on west-northwest directed slip (Fig. 5.6, box 1). The inverse relationship, west-northwest superposed on north-northeast slip lineations, was documented at five locations (D2-3, D2-4, D2-5, D2-6, D2-7) (Fig. 5.6, box 2). Faults striking north-northwest to north-northeast will move right-oblique in the west-northwest extensional field, and left-oblique when slip is associated with north-northeast extension. When the fault strike is oriented east-northeast (Fig. 5.6, stereonet D2-6a) then slip associated with north-northeast extension becomes right-lateral to right-oblique and west-northwest directed slip has a

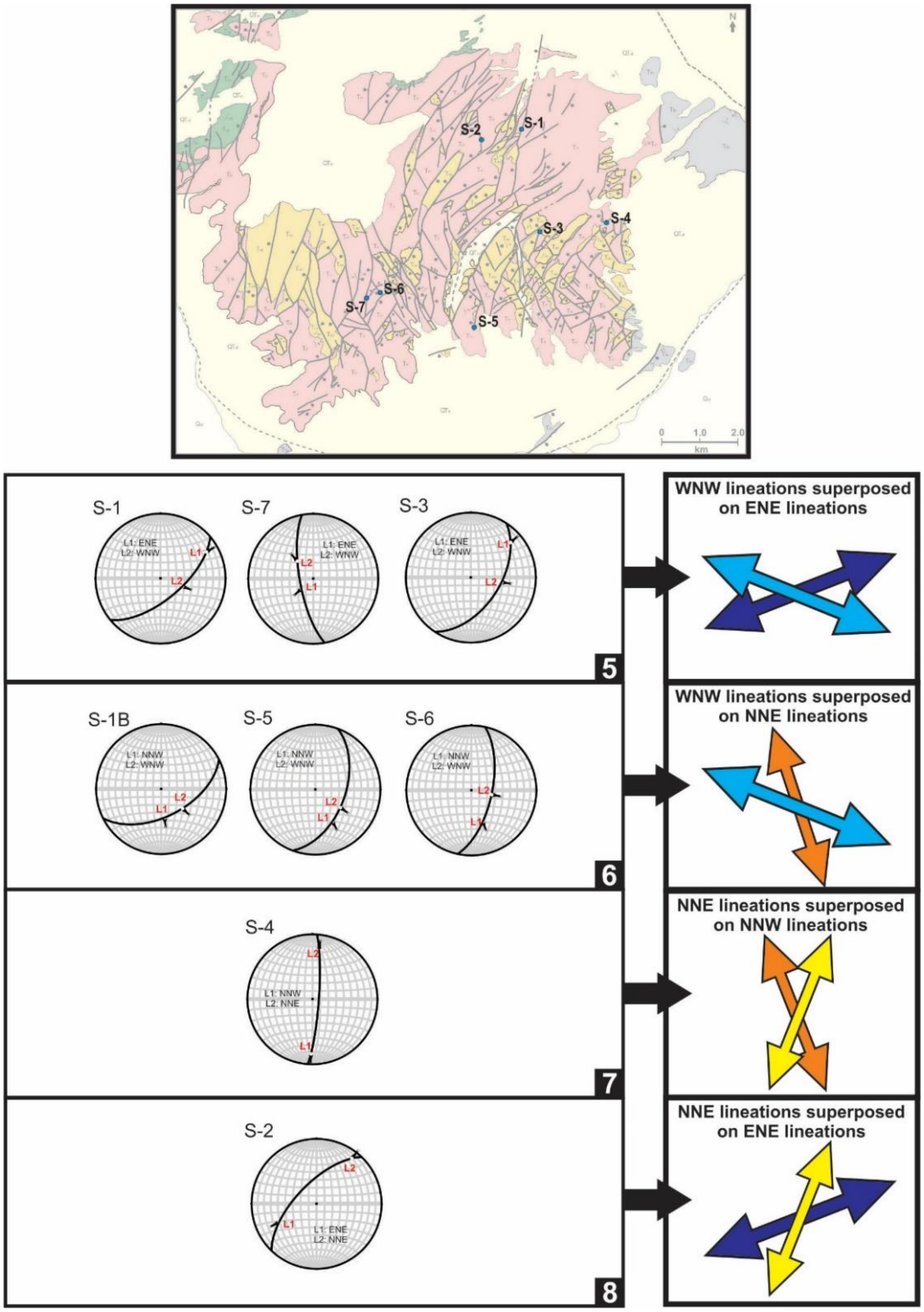

Figure 5.4. Stereonets displaying superposed lineations, which demonstrate two separate periods of flatting strain. Numbers above individual stereonets can be geographically located on the geologic map above. To the right of the stereonets, a schematic representation of what the stereonet data reveals. Color highlights similar directions of extension.

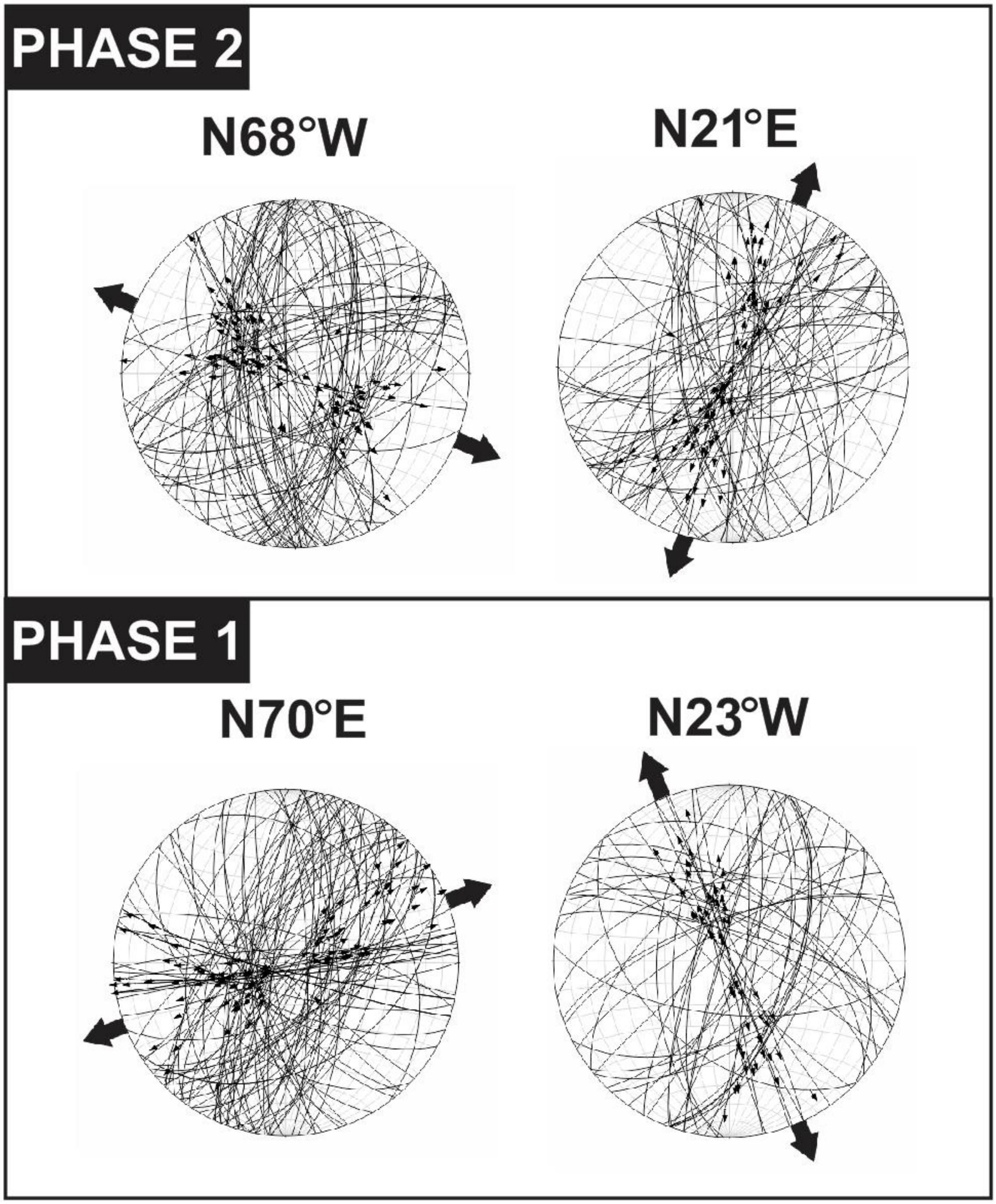

Figure 5.5. Schmidt equal-area lower hemisphere stereographic projections of fault kinematic data separated in homogeneous kinematic families.

left-oblique sense of movement. The angle between incompatible slickenlines on fault surfaces varies but is generally within 75-90 degrees from one another.

Rose diagrams were generated for fault plane population measurements taken at the outcrop scale to analyze if any orientation was preferred for differing extension directions using Stereonet 7 designed by Allmendinger (Fig. 5.7 1a. and 1b). Faults grouped into the west-northwest kinematic axis group has a clear preferred strike orientation of north-northwest and a secondary preference of movement on northeast striking planes, whereas the inverted relationship can be seen for measurements grouped in the north-northeast extensional family.

There is a clear relationship between preferred fault orientation and the direction in which space is accommodated in the crush zones of major faults. However, Fig. 5.7 2a. and 2b., demonstrates the same relationship is not represented at map scale with over 60% of west-northwest and north-northeast extending fault slip measurements associated with faults with a north-northeast to northeast map trace. To gain a better understanding of the orthogonal symmetry of fault orientations in the Phase Two extensional regime, west-northwest and north-northeast kinematic groups were combined and poles to planes were generated using Allmendinger's Stereonet program. In the diagram four point maxima, indicated by the yellow and light green areas, oriented east-northeast, west-southwest, northwest and southeast are present with an orthorhombic symmetry (Fig. 5.8 a).

5.1.2 Phase One – Mutually Cross-cutting East-northeast and North-northwest Slip Lineations

Mutually cross-cutting fault slip measurements associated with phase one kinematics was documented in five locations in the SVH (Fig. 5.9). In three locations, (D1-1, D1-3, and D1-5) north-northwest oriented slip superposes east-northeast slip. The reverse relationship was documented in two locations (D1-2 and D1-4) and east-northeast is superposed on north-northwest. The direction of slip varies with change in the orientation of the fault plane. Northwest striking faults have right-oblique movement in an east-northeast extensional field and left-lateral motion in north-northwest extension (Fig. 5.9, stereonet D1-1). On north-northeast striking faults (Fig. 5.9, stereonet D1-3 and D1-5), east-northeast extension has left-oblique sense of slip, and a right-oblique sense of slip is associated with north-northwest extension. Northeast oriented faults (Fig. 5.9, stereonet D1-2) have left-lateral slip and pure dip-slip associated with east-northeast and west north-west extension, respectively. The angle between incompatible slip lineations varies from 60-95 degrees on individual fault planes.

Rose diagrams were generated for phase one fault plane population measurements taken at the outcrop scale to analyze if any orientation was preferred (Fig. 5.7, 1c and 1d). Faults grouped into the east-northeast kinematic axes family have a clear preferred strike orientation of north-northeast, whereas striae group in the north-northwest extensional family have a preference to slip on north-northeast trending faults. Fig. 5.7, stereonets 2c and 2d, demonstrates the preference for faults extending east-northeast to slip on north-northeast striking faults is consistent with fault traces at map scale. The relationship between north-northwest extending

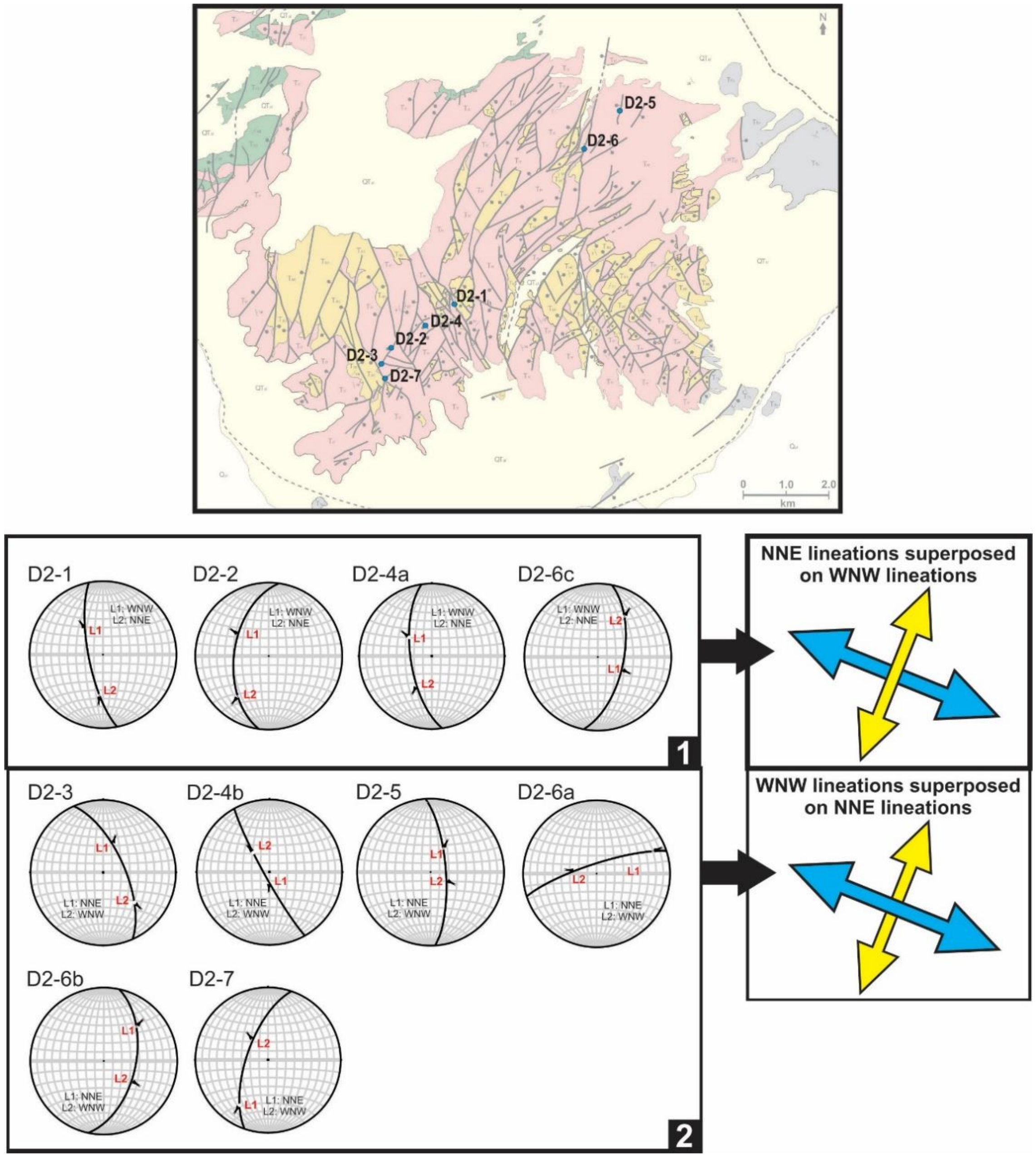

Figure 5.6. Stereonets demonstrating mutually cross-cutting lineations. Box 1 shows stereographic projections of north-northeast lineations superposed on west-northwest lineations, and Box 2 shows the inverted relationship (west-northwest superposed on north-northeast striae).

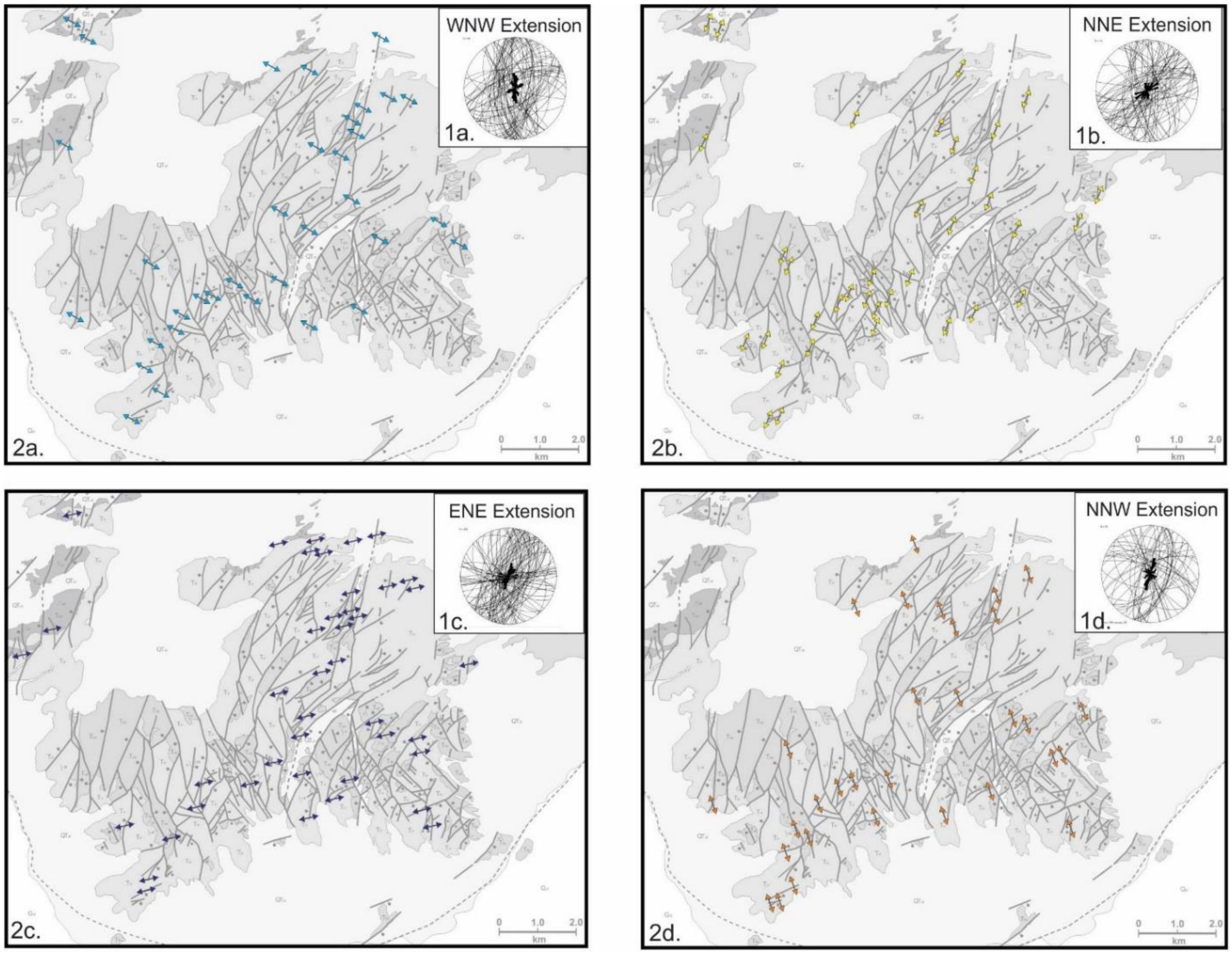

Figure 5.7. Extensional axes maps of each extension direction with rose diagrams in the upper right hand corner demonstrating the preferred orientation of fault populations. Top pair represent Phase 2, bottom represent the earlier Phase 1 of deformation.

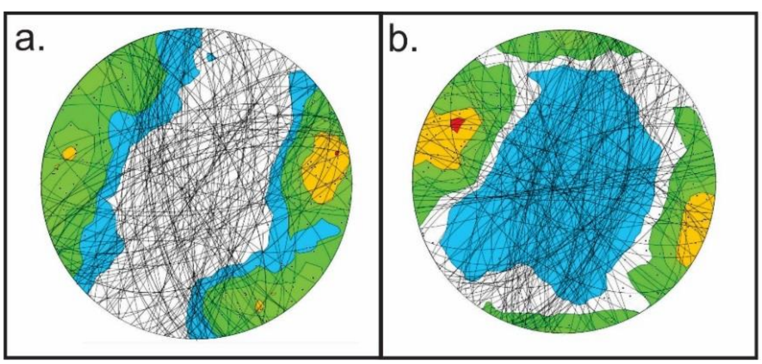

Figure 5.8. Contour of poles to fault planes showing four different orientations of faults creating orthorhombic symmetry. a) Phase 2 and b) Phase 1. Warmer tones represent higher density of measurements.

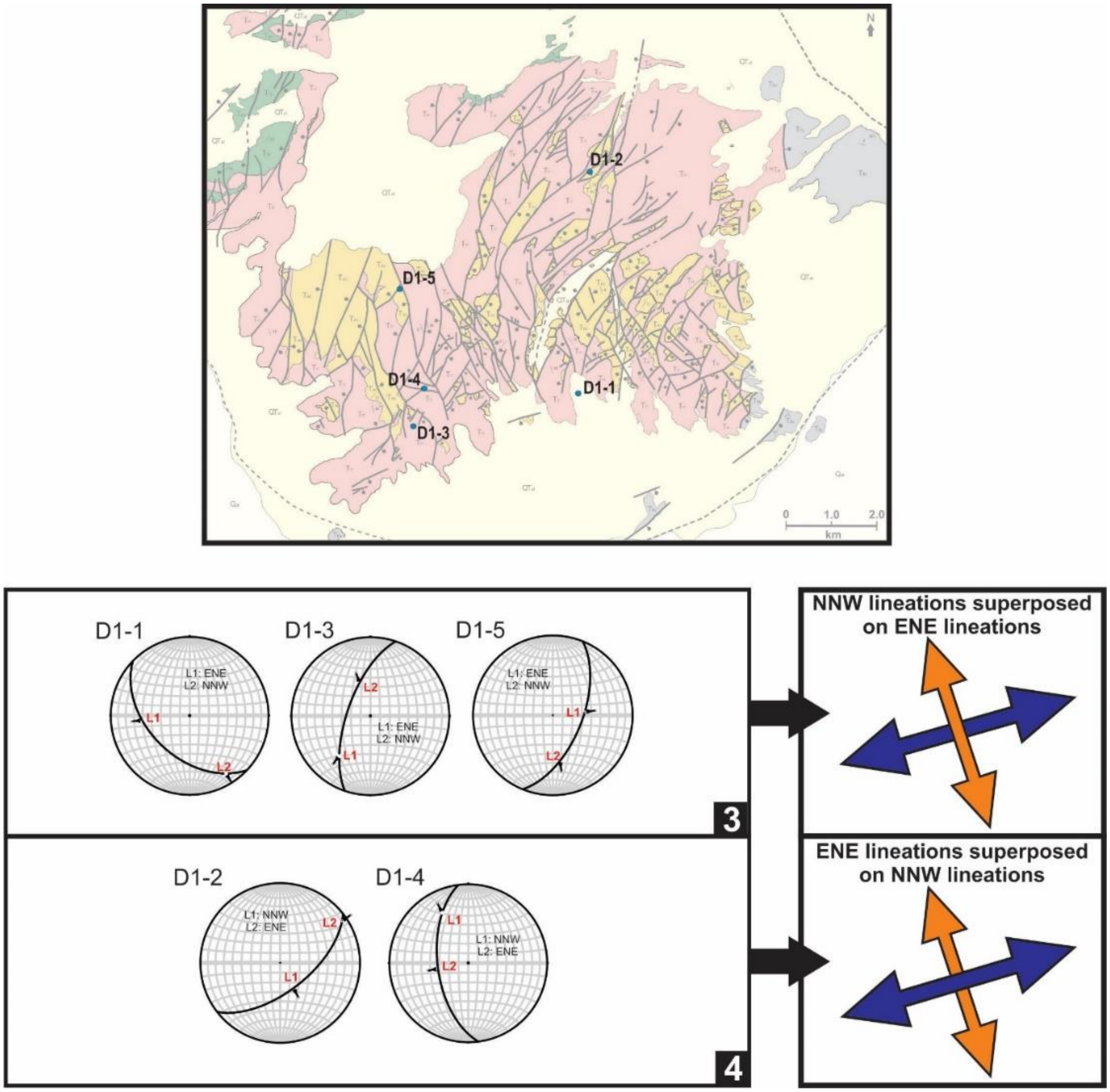

Figure 5.9. Stereonets demonstrating mutually cross-cutting lineations. Box 1 shows stereographic projections of north-northwest lineations superposed on east-northeast lineations, and Box 2 shows the inverted relationship (east-northeast superposed on north-northwest striae).

fault slip measurements is not as apparent and at map scale are accommodated on faults striking primarily northeast and north-northwest. To gain a better understanding of the symmetry of fault orientations in phase 2 deformation, east-northeast and north-northwest kinematic families were combined and poles to planes were generated. In the diagram four distinct point maxima oriented west-northwest, east-southeast, north-northeast, and south-southeast are clear Fig. 5.8 b).

5.2 Primary and Secondary Axes Determination

Primary and secondary strain axes for the two separate phases of mutually cross-cutting slip lineations is determined by GPS and focal mechanism data and thickness variations across expected active fault orientations. Modern day extension in the region (west-northwest) is well documented based on earthquake focal mechanism and GPS velocity data, and was used to define the primary extension axes in the phase 2 mutually cross-cutting event (west-northwest and east-northeast). Secondary strain axes of similar north-northeast orientations have been documented in the northern extent of the Mina deflection (Ferranti et al., 2009) and in the CWL, a strain meter recorded short-period cyclicity in strain-axis orientations between a primary and secondary extension direction, northwest and north-northeast respectively (Ryall and Priestley, 1975). Determining primary and secondary strain axes for the phase one mutually cross-cutting event (east-northeast and north-northwest) is more problematic due to fault slip measurements reflecting ancient earthquakes which cannot be verified with modern day movement. However, thickening across north-northeast striking faults in a westward direction indicate majority of accommodation was made on faults moving in east-northeast extension (Fig. 3.4). Based on the compatibility criteria listed above and slip superposition relationships we documented four extension directions (N68°W, N21°E, N70°E, and N23°W) separated into two successive periods with a primary and secondary strain axes, each characterized by mutually cross-cutting slip relations in the SVH.

CHAPTER 6

DISCUSSION

The geometry of structures in the SVH are of particular importance for the reason it is geographically located within in the hanging wall of the curved EPFZ. Analogous to the SVH, geometries and basin development in curved fault systems of the northern extent of the Mina deflection, including RSM basin, have documented finite flattening characterized by mutually cross-cutting fault slip lineations. Several models have accounted for a discrepancy in slip vectors, however in areas of non-plane strain, as in the CWL and ECSZ, typical plane strain models do not work, which led Ferranti (2009) to the conclusion of finite flattening. The central issue surrounding this model is whether finite flattening is a geometric requirement for movement and basin development in a kinematically linked curved fault system. If so are there other geometries which can also create the same strain phenomena. The geologic investigation of the SVH and surrounding faults presented here provides the constraints needed to evaluate how extensional structures accommodate space in a curved fault system and whether other fault geometries may also be a factor in localized areas of finite flattening.

Multiple fault orientations typically are explained as being related to different phases of deformation. Typical Andersonian mechanics focuses on the fracturing of rocks using Coulombs failure and only accounts for two conjugate sets of fault orientations both inclined at 45°to the direction of maximum compression. This model of thinking does not account for multiple faults with simultaneous movement as seen in the SVH and in other areas surrounding the Mina deflection. Reches (1983) carried out experiments which showed three or four sets of faults arranged with orthorhombic symmetry, and an equal number of slip directions, was needed to accommodate space in areas of triaxial deformation. In the SVH the presence of multiple fault sets with orthorhombic symmetry (Fig. 5.8) and the presence of mutually cross-cutting lineations leads us to the interpretation that triaxial deformation and specifically flattening strain was present during the late Cenozoic.

The reconciliation of fault-slip compatibility and superposition data in the SVH demonstrates that displacement is accommodated by significant internal deformation of the hanging wall block during two separate periods of finite flattening. The most modern event (phase 2) is characterized by mutually cross-cutting west-northwest and north-northeast slip lineations which superposes an older history of east-northeast and north-northwest mutually cross-cutting slicknelines (phase 1). Phase two directions of extensional strain are distinguished as primary (west-northwest) and secondary (north-northeast) on the basis of modern day seismology and contemporary global positioning system (GPS) velocities (Unruh et al., 2003; Oldow, 2003). The data from a strain meter recorded north of RMS (Ryall and Priestley,1975) verifies two extension directions are occurring in short cyclic periods. Phase one finite flattening has primary (east-northeast) and secondary (north-northwest) strain axes and are determined from an increase in thickness from 200 m to 600 m of Rhyolite Ridge tuff over a single north-northeast striking down to the west fault (Fig. 3.5, C-C’, bolded black fault). The thickness increase across north-northeast striking faults in an east-west direction, indicate more accommodation was made as west-northwest movement occurred as opposed to north-northwest. In the western Volcanic Hills sandstone dikes also record a mutually cross-cutting relationship in the Silver Peak Formation attributed to upper plate movement on the underlying detachment fault (Ridde, 2018).

The geometry of late Cenozoic structures creates boundary conditions which impact how the hanging wall block will internally deform as normal movement occurs. Ferranti et. al (2009), in RSM was able to demonstrate large magnitude extension in a curved faults system caused the hanging wall block to diverge during displacement which resulted in finite flattening (Fig. 6.1).

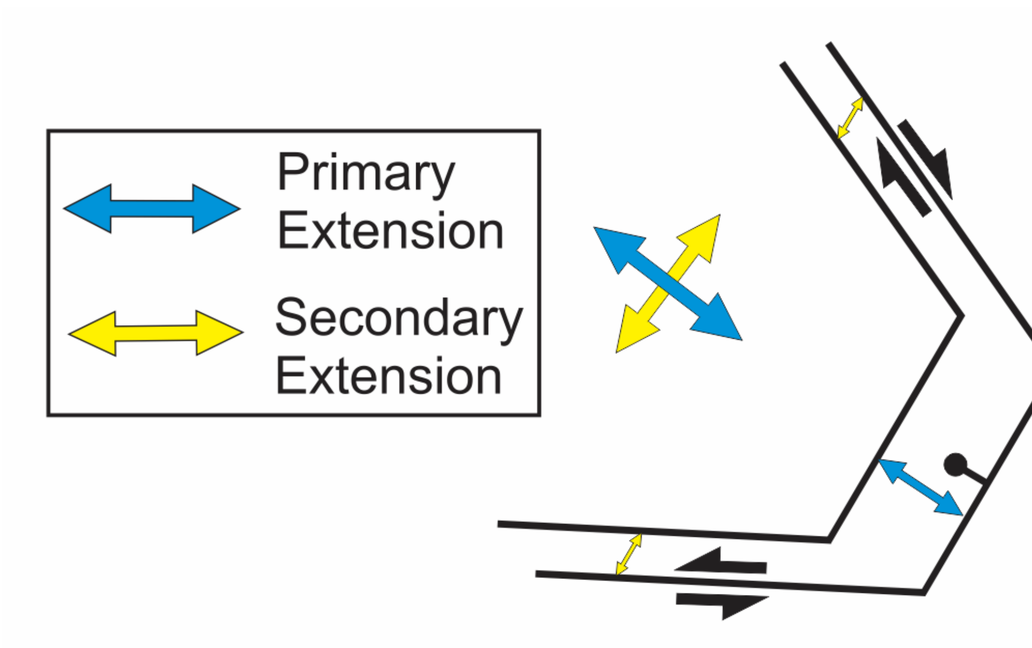

Figure 6.1. Rectilinear schematic representation of two simultaneous extension directions with mutually cross-cutting slip lineations which form due to a space problem in a curved fault geometry

The study documented mutually cross-cutting slip lineations on structures which accommodated a primary and secondary direction of movement formed as discrete episodes. The SVH located in the hanging wall of the curved EPFZ is analogous to the geometry of RSM and mutually cross-cutting slip lineations are recorded. However, in the SVH, two sets of mutually cross-cutting lineations superposed are present (west-northwest and north-northeast superposed on east-northeast and north-northwest) indicating two distinct episodes of flattening strain have occurred.

Fault-slip data in the eastern extent of the SPR, measured on the faults of the EPFZ, record only west-northwest extension in the Fish Lake Valley assemblage. Ng (2017) was able to document based on a high resolution gravity line, spanning from the central SPR to the eastern portion of the SVH, that high-angle faults which controlled deposition of the Coyote Hole Group (13-4 Ma), soled into the detachment, and were later reactivated, including the EPFZ. The high-angle faults cut the detachment and provided accommodation space for the deposition of Fish Lake Valley assemblage at ~4Ma, during west-northwest extension. With the absence of east-northeast, north-northwest, and north-northeast extension and the presence of west-northwest extension measured on the rocks of Fish Lake Valley assemblage in the western flank of the SPR, we can infer phase two flattening strain (west-northwest and north-northeast) occurred after 4 Ma coincident with the onset of the curved EPFZ analogous with the geometry of RSM.

Thickness variation of the Coyote Hole group across high-angle faults in the SVH confirms movement on the detachment was occurring prior to 4Ma. Mutually cross-cutting fault-slip lineations (ENE and NNW) predate the modern west-northwest and north-northeast extensional event associated with the curved fault geometry of the EPFZ. Phase one finite flattening cannot be attributed to the same geometry and occurred as westward translating movement on the detachment disarticulated the upper plate rocks. Flattening strain attributed to detachment faults is not fully understood and more research must be done to fully realize the geometric space problem causing triaxial deformation.

CHAPTER 7

CONCLUSION

The southeastern Volcanic Hills has four observed extensional directions N68°W, N21°E, N70°E, and N23°W. Two sequential periods of flattening strain have occurred. The most recent (phase two) is demonstrated by west-northwest (primary) and north-northeast (secondary) mutually cross-cutting slickenside lineations and is a result of a space problem created by down to the west movement on the curved Emigrant Peak fault zone which initiated at ~ 4 Ma (Fig. 7.1 c.). The first phase is demonstrated by east-northeast (primary) and north-northwest (secondary) mutually cross-cutting fault striae, coincident with the synextensional deposition of the Coyote Hole Group as westward translating movement on the Silver Peak Lone Mountain detachment occurred from the mid to late Miocene (Fig. 7.1 b.).

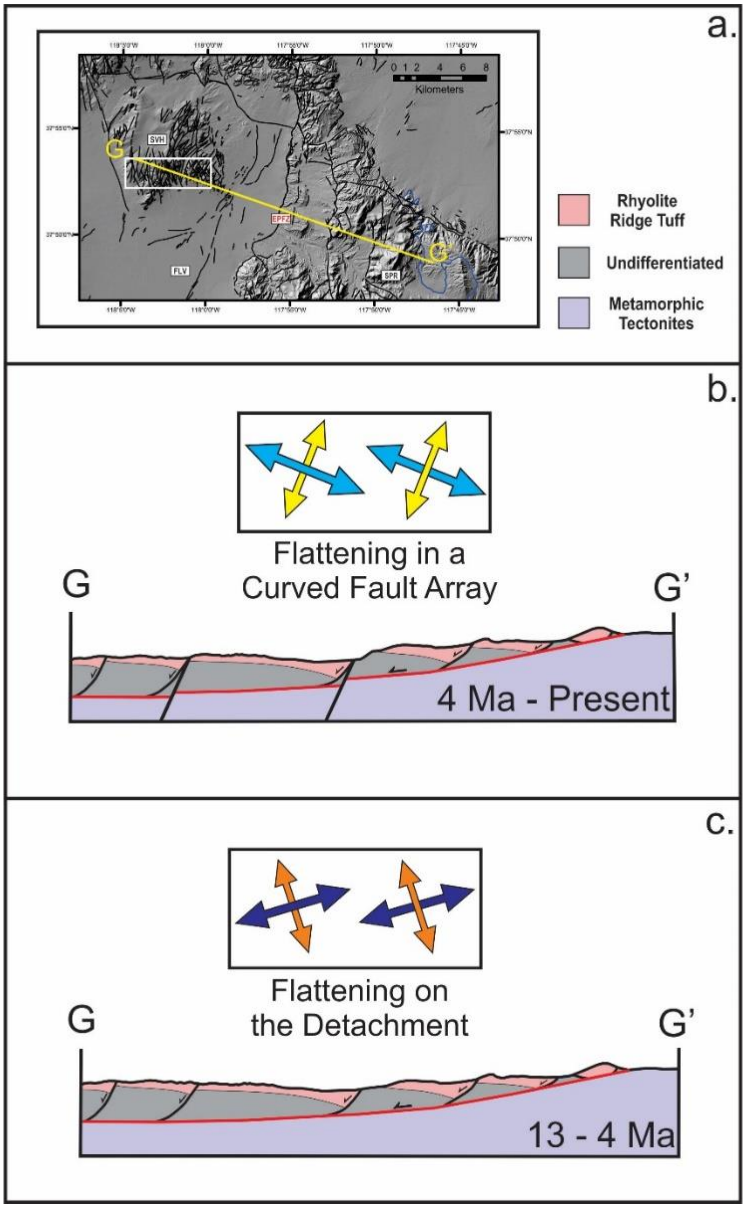

Figure 7.1. Hillshade of the northern FLV including SVH and SPR. G-G' represents drafted cross sections. b. cross section of fault geometry during phase two flattening strain where high angel faults cut the detachment. c. cross section of phase one geometry showing high angel faults which sole into the detachment fault creating space for the deposition of the Coyote Hole Group.

REFERENCES

Allmendinger, R. W., Cardozo, N. C., and Fisher, D., 2012, Structural Geology Algorithms: Vectors & Tensors: Cambridge, England, Cambridge University Press, 289 pp.

Anderson, E. M., 1951, The dynamics of faulting and dyke formation with applications to Brittain: Edinburgh, Oliver & Boyd, 206 p.

Angelier, J., 1984, Tectonic analysis of fault slip data sets: Journal of Geophysical Research, v. 89, p. 5835-5848.

Angelier, J., 1985, Extension and rifting: the Zeit region, Gulf of Suez: Journal of Structural Geology, v. 7, p. 605-611.

Argus, D.F., and Gordon, R.G., 1991, Current Sierra Nevada–North America motion from very long baseline interferometry: Implications for the kinematics of the western United States: Geology, v. 19, p. 1085–1088

Bellier, O., and Zoback, M.L., 1995, Recent state of stress change in the Walker Lane zone western Basin and Range Province, United States: Tectonics, v. 14, p. 564–593, doi: 10.1029/94TC00596.

Bennett, R.A., Wernicke, B.P., Niemi, N.A., Friederich, A.M., and Davis, J.L., 2003, Contemporary strain rates in the northern Basin and Range Province from GPS data: Tectonics, v. 22, p. 3-1–3-31.

Dixon, T.H., Miller, M., Farina, F., Wang, H., and Johnson, D., 2000, Presentday motion of the Sierra Nevada block and some tectonic implications for the Basin and Range Province, North American Cordillera: Tectonics, v. 19, p. 1–24.

Doser, D.L., 1988, Source mechanisms of earthquakes in the Nevada seismic zone (1915–1943) and implications for deformation in the western Great Basin: Journal of Geophysical Research, v. 93, p. 15,001–15,015, doi: 10.1029/JB093iB12p15001.

Ferranti, L., Oldow, J. S., Geissman, J. W., Nell, M. M., 2009, Flattening strain during coordinated slip on a curved fault array, Rhodes Salt Marsh extensional basin, central Walker Lane, west-central Nevada: Geological Society of America Special Paper 447, p. 189-213.

Hardyman, R.F., and Oldow, J.S., 1991, Tertiary tectonic framework and Cenozoic history of the central Walker Lane, Nevada, in Raines, G.L., Lisle, R.E., Schafer, R.W., and Wilkinson, W.H., eds., Geology and Ore Deposits of the Great Basin: Reno, Nevada, Geological Society of Nevada, Symposium Proceedings, p. 279–301.

Kistler, R. W., 1991, Chemical and isotopic characteristics of plutons in the Great Basin, in Raines, G.L., et al., eds., Geology and ore deposits of the Great Basin: Reno, Geologic Society of Nevada, p. 107-110.

Kirsch, S.A., 1971, Chaos structure and turtleback dome, Mineral Ridge, Esmeralda County, Nevada: Geological Society of America Bulletin, v. 82, p. 3169–3176

Kohler, G., 1994, Structural evolution of metamorphic tectonites beneath the Silver Peak–Lone Mountain detachment fault, west-central Nevada [M.S. thesis]: Houston, Texas, Rice University, p.126.

Lee, J., Stockli, D.F., Owen, L.A., Finkel, R.C., and Kislitsyn, R., 2009a, Exhumation of the Inyo Mountains, California: Implications for the timing of extension along the western boundary of the Basin and Range Province and distribution of dextral fault slip rates across the eastern California shear zone. Tectonics, v. 28, TC1001, doi:10.1029/2008TC002295

Marrett, R., and Allmendinger, R. W., 1990, Kinematic analysis of fault-slip data: Journal of Structural Geology, v. 12, no. 8, p. 973-986.

McKee, E. H., 1968, Age and rate of movement on the northern part of the Death Valley-Furnace Creek Fault Zone, California: Geological Society of America Bulletin, v. 79, p. 509-512.

Miller, M.M., Johnson, D.J., Dixon, T., and Dokka, R.K., 2001, Refined kinematics of the Eastern California shear zone from GPS observations, 1993–1998: Journal of Geophysical Research, v. 106, p. 2245–2264.

Mueller, N., Oldow, J.S., Katopody, D., Gibson, K., Pham, B., McBride, K., Shilpakar, P., and Aguilar, R., 2016, Pliocene reorganization of eastern California shear zone kinematics documented in the Cucomungo Canyon restraining bend of the Furnace Creek-Fish Lake Valley fault zone, northern Death Valley and southern Fish Lake Valley, California, western Great Basin, Geological Society of America Abstracts with Programs, v. 48, no. 4, doi: 10.1130/abs/2016CD-274477.

Ng, M., and Oldow, J.S., 2017, Geometry of superposed low-angle detachment and high-angle faults in the western Silver Peak Range and northern Fish Lake Valley, Nevada, Geological Society of America Abstracts with Programs, v. 49, no. 6, doi: 10.1130/abs/2017AM-306721.

Oldow, J. S., 1992, Late Cenozoic Displacement Partitioning in the Northwestern Great Basin: Structure, Tectonics, and Mineralization of the Walker Lane, Stewart, J., ed., Walker Lane Symposium Proceedings Volume, Geological Society of Nevada, Reno, NV, p. 17-52.

Oldow, J.S., Kohler, G., and Donelick, R., 1994, Late Cenozoic extensional transfer in the Walker Lane strike-slip belt, Nevada: Geology, v. 22, p. 637–640

Oldow, J.S., Aiken, C.L.V., Ferguson, J.F., Hare, J.L., and Hardyman, R.F., 2001, Active displacement transfer and differential motion between tectonic blocks within the central Walker Lane, western Great Basin: Geology, v. 29, p. 19–22, doi: 10.1130/0091 7613(2001)029<0019:ADTADB> 2.0.CO;2.

Oldow, J. S., 2003, Active transtensional boundary zone between the western Great Basin and Sierra Nevada block, western U.S. Cordillera: Geological Society of America, v. 31, no. 12, p. 1033-1036.

Oldow, J. S., Geissman, J. W., and Stockli, D. F., 2008, Evolution and Strain Reorganization within Late Neogene Structural Stepovers Linking the Central Walker Lane and Northern Eastern California Shear Zone, Western Great Basin: International Geology Review, v. 50, p. 270-290.

Oldow, J. S., Elias, E. A., Ferranti, L., McClelland, W. C., and McIntosh, W. C., 2009, Late Miocene to Pliocene synextensional deposition in fault-bounded basins within the upper plate of the western Silver Peak-Lone Mountain extensional complex, west-central Nevada: Geological Society of America Special Paper 447, p. 275-312.

Oldow, J.S., Katopody, D.T., Kerstetter, S.R., and Mueller, N.J., 2016, Regional setting, geometry, and structure of the northern Fish Lake Valley basin: https://mk0americanlithp450n.kinstacdn.com/wp-content/uploads/2018/05/American-Lithium-Report.pdf (accessed October 2018).

Petronis, M. S., Geissman, J. W., Oldow, J. S., and McIntosh, W. C., 2009, Late Miocene to Pliocene vertical-axis rotation attending development of the Silver Peak-Lone Mountain displacement transfer zone, west-central Nevada in Oldow, J.S., and Cashman, P.H., eds., Late Cenozoic structure and evolution of the Great Basin-Sierra Nevada transition: 190 Geological Society of America

Petit, J. P., 1987, Criteria for the sense of movement on fault surfaces in brittle rocks: Journal of Structural Geology, v. 9, no. 5/6, p. 597-608.

Reches, Z., 1983, Faulting of rocks in three-dimensional strain fields: II. Theoretical analysis: Tectonophysics, v. 95, p. 133-156.

Reheis, M.C., 1991, Geologic Map of Late Cenozoic Deposits and Faults in the Western Part of the Rhyolite Ridge 15 Minute Quadrangle, Esmeralda County, Nevada: U.S. Geological Survey Miscellaneous Investigations Series Map I-2183, scale 1:24,000.

Reheis, M.C., Slate, J.L., Sarna-Wojcicki, A.M., and Meyer, C.C., 1993, A late Pliocene to middle Pleistocene pluvial lake in Fish Lake Valley, Nevada and California: Geological Society of America Bulletin, v. 105, p. 953-967, doi: 10.1130/0016-7696(1993)105<0953: ALPTMP>2.3.CO; 2.

Reheis, M. C., and Sawyer, T. L., 1997, Late Cenozoic history and slip rates of the Fish Lake Valley, Emigrant Peak, and Deep Springs fault zones, Nevada and California: Geological Society of America Bulletin, v. 109, no. 3, p. 280-299.

Ridde, A., 2018, Strain implications for the formation of clastic dikes during synextensional deposition of Miocene volvanoclastic rocks in the Volcanic Hills, southwest Nevada [M.S. thesis]: University of Texas at Dallas, 48 p.

Robinson, P.T., McKee, E.H., and Moiola, R.J., 1968, Cenozoic volcanism and sedimentation, Silver Peak region and adjacent California *in* Geological Society of America Memoirs, v. 116, p. 577-612.

Robinson, P. T., Stewart, J. H., Moiola, R. J., and Albers, J. P., 1976, Geologic map of the Rhyolite Ridge Quadrangle, Esmeralda County, Nevada: U. S. Geological Survey Geologic Quadrangle Map GQ-1325, scale 1:62,500.

Rogers, A.M., Harmsen, S.C., Corbett, E.J., Priestley, K., and dePolo, D., 1991, The seismicity of Nevada and some adjacent parts of the Great Basin, in Slemmons, D.B., Engdahl, E.R., Zoback, M.D., and Blackwell, D.D., eds., Neotectonics of North America: Boulder, Colorado, Geological Society of America, Decade Map Volume 1, p. 153–184.

Ryall, A., and Priestley, K., 1975, Seismicity, secular strain, and maximum magnitude in the Excelsior Mountains area, western Nevada and eastern California, Geological Society of America Bulletin, v. 86, p. 1585-1592.

Snow, J. K., and Wernicke, B., 1989, Uniqueness of geologic correlations: an example from the Death Valley extended terrain: Geological Society of America Bulletin, v. 101, p. 1351-1362.

Speed, R. C., and Cogbill, A. H., 1979, Cenozoic volcanism of the Candelaria region, Nevada: Geological Society of American Bulletin, Part II, v. 90, p. 456-493.

Stewart, J. H., 1967, Possible large right-lateral displacement along fault and shear zones in the Death Valley-Las Vegas area, California and Nevada: Geological Society of America Bulletin, v. 78, p. 131-142.

Stewart, J. H., and Diamond, D. S., 1990, Changing patterns of extensional tectonics; Overprinting of the basin of the middle and upper Miocene Esmeralda Formation in western Nevada by younger structural basins: Geological Society of America Memoir 176, 28 p.

Stockli, D.F., Dumitru, T.A., McWilliams, M.O., and Farley, K.A., 2003, Cenozoic tectonic evolution of the White Mountains, California and Nevada: Geological Society of America Bulletin, v. 115, no. 7, p. 788–816

Tincher, C. R., and Stockli, D. F., 2009, Cenozoic volcanism and tectonics in the Queen Valley area, Esmeralda County, western Nevada Nevada *in* Oldow, J.S., and Cashman, P.H., eds., Late Cenozoic structure and evolution of the Great Basin-Sierra Nevada transition: Geological Society of America Special Paper 447, p. 255-274.

Unruh, J., Humphrey, J., and Barron, A., 2003, Transtensional model for the Sierra Nevada frontal fault system, eastern California: Geology, v. 31, p. 327–330.

Walker, J.D., Bidgoli T.S., Didericksen, B.D., Stockli D.F., and Andrew, J.E., 2014, Middle Miocene to recent exhumation of the Slate Range eastern California, and implications for the timing of extension and the transition to transtension: Geologic Society of America, v.10, no. 10, p. 276-291

Wesnousky, S.G., 2005, Active faulting in the Walker Lane: Tectonics, v. 24, p. TC3009

Zoback, M.L., 1989, State of stress and modern deformation of the northern Basin and Range Province: Journal of Geophysical Research, v. 94, p. 7105-7128.

BIOGRAPHICAL SKETCH

Amy Rachelle Webber was born in Nashville, Tennessee and earned a Bachelor of Science in Geosciences from The University of Texas at Dallas in Summer 2015. Amy fast-tracked into her master's program at The University of Texas at Dallas and began her thesis work in structural geology under Dr. John S. Oldow that same summer.

CURRICULUM VITAE

Amy Webber

800 W Campbell Rd, Richardson TX, 75080
University of Texas at Dallas, Department of Geosciences, ROC 21

Education

Master of Science (M.S.) in Geosciences
The University of Texas at Dallas
Fall 2016 – Fall 2018

Bachelor of Science (B.S.) in Geosciences, Cum Laude with Major Honors
The University of Texas at Dallas
Fall 2014 – Summer 2017

Research and Experience

Graduate Research Assistant, UT Dallas, Dept. of Geosciences
Summer 2015 – Spring 2017

Geoscience Intern, Pioneer Natural Resources
Summer 2016